

FORM EG&G-398
(Rev. 05-79)

THIS DOCUMENT CONTAINS
POOR QUALITY PAGES

INTERIM REPORT

Accession No. _____
Report No. EGG-TFBP-5209

Contract Program or Project Title:
Thermal Fuels Behavior Program

Subject of this Document:
Feasibility Analysis for the SUPER-SARA Small Break LOCA/Flow Starvation Test Program

Type of Document:
Analysis

Author(s):
J. M. Broughton, G. T. Liu, R. W. Garner

Date of Document:
July 1980

Responsible NRC Individual and NRC Office or Division:
M. L. Picklesimer, Reactor Safety Research

This document was prepared primarily for preliminary or internal use. It has not received full review and approval. Since there may be substantive changes, this document should not be considered final.

EG&G Idaho, Inc.
Idaho Falls, Idaho 83401

Prepared for the
U.S. Nuclear Regulatory Commission
Washington, D.C.
Under DOE Contract No. DE-AC07-76ID01570
NRC FIN No. A6041

INTERIM REPORT

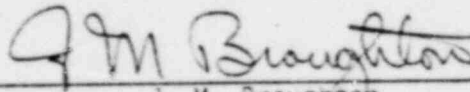
NRC Research and Technical
Assistance Report
8008180579

June 1980


FEASIBILITY ANALYSIS FOR THE
SUPER-SARA SMALL BREAK
LOCA/FLOW STARVATION TEST PROGRAM

J. M. Broughton
G. T. Liu
R. W. Garner

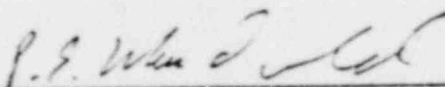
Approved:



J. M. Broughton
PBF Experiment Specification and Analysis Branch



R. K. McCardell, Manager
PBF Experiment Specification and Analysis Branch



P. E. MacDonald, Manager
LWR Fuel Research Division

THERMAL FUELS BEHAVIOR PROGRAM
EG&G Idaho, Inc.

CONTENTS

1.	INTRODUCTION	1
2.	EXPECTED SYSTEM THERMAL-HYDRAULIC AND FUEL ROD RESPONSE DURING A SMALL BREAK LOCA TRANSIENT	3
3.	OBJECTIVES OF THE SUPER-SARA SMALL BREAK LOCA TESTS	4
4.	SUPER-SARA TEST FACILITY	6
5.	THE TRAC-BDO COMPUTER CODE AND MODEL FOR APPLICATION TO SUPER-SARA	9
5.1	General Description of TRAC	9
5.1.1	TRAC Characteristics	9
5.1.2	Physical Phenomena Treated	10
5.2	Description of TRAC-BDO Code	10
5.3	TRAC-BDO Model for SUPER-SARA	11
6.	TRAC-BDO CALCULATIONS FOR SUPER-SARA SMALL BREAK LOCA TRANSIENTS	16
6.1	Steam Atmosphere Test Conditions	16
6.2	Steam/Water Test Conditions	26
7.	CONCLUSIONS	41
	REFERENCES	42
	APPENDIX A: TRAC-BDO CALCULATED SYSTEM AND FUEL ROD VARIABLES . .	43
	APPENDIX B: METHOD USED FOR CALCULATING LUMPED PARAMETER HEAT TRANSFER COEFFICIENT FOR THE SUPER-SARA SMALL BREAK TEST GEOMETRY	47

FIGURES

1.	Vertical cross section of the SUPER-SARA in-pile test section (36 rods).	7
2.	Horizontal cross section of SUPER-SARA test section	8
3.	Horizontal cross section of SUPER-SARA test section showing the components modeled in TRAC	13
4.	TRAC axial nodalization and the axial power distribution . . .	14
5.	Fuel rod groups in the SUPER-SARA test bundle.	15

FIGURES

6.	Map of calculated cladding peak temperatures as a function of linear peak power and steam flow rate.	18
7.	Calculated cladding peak temperatures in the SUPER-SARA test bundle at 0.31 kW/m linear peak power, and 0.3 and 0.5 m/s steam flow	19
8.	Cladding peak, steam, and shroud inside surface temperatures versus time for the calculation of high cladding temperature (~ 2400 K) with steam cooling	21
9.	Fuel rod and shroud inside surface heat flux from the different heat transfer modes versus time for the calculation of high cladding temperature (~ 2400 K) with steam cooling	22
10.	Cladding, steam, and shroud inside surface temperatures versus elevation for the calculation of high cladding temperature (~ 2400 K) with steam cooling	23
11.	Rod surface heat flux, metal/water reaction heat flux, oxide thickness, and peak-to-average rod power versus axial elevation for the calculation of high cladding temperature (~ 2400 K) with steam cooling	24
12.	Heat transfer regimes modeled by TRAC-BDO at low inlet coolant flow	28
13.	Calculated cladding peak temperatures as a function of both coolant mass flow and linear peak power for steam/water	30
14.	Map of collapsed water level within the bundle as a function of coolant mass flow and linear peak power	31
15.	Calculated fuel rod peak temperatures in the SUPER-SARA test bundle at 15.75 and 22.64 kW/m, and 0.2 kg/s	32
16.	Calculated cladding peak, steam, and shroud inside surface temperatures versus time for the calculation of high cladding temperature with steam/water conditions	34
17.	Fuel rod surface heat flux via convection and radiation versus time for the steam/water case at the peak cladding temperature elevation	35
18.	Cladding metal-water reaction heat flux and oxide layer thickness versus time for the steam/water case at the cladding peak temperature elevation	37
19.	Calculated cladding surface, fuel centerline, steam and shroud inside surface temperatures versus axial elevation	38

FIGURES

20. Cladding surface heat transfer coefficients versus axial elevation for the different heat transfer modes and the bundle void fraction 40

TABLES

1. Fuel Rod Characteristics 6

FEASIBILITY ANALYSIS FOR THE SUPER-SARA SMALL
BREAK LOCA/FLOW STARVATION TEST PROGRAM

1. INTRODUCTION

The SUPER-SARA Test program,¹ will be performed in the ESSOR reactor at Ispra, Italy, to study LWR fuel rod behavior during loss-of-coolant accident (LOCA) conditions. The proposed tests will evaluate fuel behavior during conditions ranging from small break LOCAs, similar to that which occurred during the TMI-2² accident, to a hypothetical PWR double-ended cold leg break LOCA, as assumed for licensing considerations. A preliminary evaluation of the feasibility of performing the proposed small break LOCA tests in SUPER-SARA is presented in this report.

Two different test conduct scenarios have been proposed to obtain the desired small break LOCA fuel behavior data. For the first set of conditions, the test bundle will initially be cooled by flowing steam. The test bundle will then be heated at a predetermined rate by fission heat. Target cladding peak temperatures are 1700 and 2300 K. The cladding heatup rate will be controlled to obtain a desired degree of cladding oxidation. The calculational objectives for this case were limited to determining the minimum power required to stabilize the cladding peak temperatures at 2300 and 1700 K with low steam flows and to determine the effect of increased inlet steam flow.

The second proposed method of conducting the small break LOCA tests would begin with the test bundle cooled by water. The transient will be initiated by reducing the bundle flow and permitting the bundle to become uncovered due to boiling. The bundle inlet flow and power will be controlled to again obtain the desired cladding peak temperatures of 1700 and 2300 K while maintaining a coolant liquid level about 1.0 m from the bottom of the bundle. Code limitations do not yet permit a totally accurate representation of this method. Instead, the calculation was initiated with the bundle water level at 1.0 m and the inlet flow and bundle power maintained constant. Bundle power and inlet flow were varied

to create a map of stabilized cladding peak temperature and bundle water level as functions of bundle power and inlet flow rate. Although the transient portion of this calculation does not reflect the actual transient that is expected to occur, these results do provide significant insight into the thermal response characteristics of the system.

A brief description of the expected fuel behavior during a small break LOCA is presented in Section 2. The specific objectives of the SUPER-SARA small break test program and the proposed test conduct are explained in Section 3, and the test facility is described briefly in Section 4. The calculations were performed with the TRAC-BCO computer code. This code and the SUPER-SARA model are discussed in Section 5. The results of the calculations are described and interpreted in Section 6. Conclusions regarding the feasibility for performing the tests are discussed in Section 7.

2. EXPECTED SYSTEM THERMAL-HYDRAULIC AND FUEL ROD RESPONSE DURING A SMALL BREAK LOCA TRANSIENT

The system conditions that result in fuel damage during a small break LOCA transient can be characterized by a slow depressurization and reduced core flow until the core is uncovered due to boiling of the coolant. As cladding temperatures increase above about 900 K because of the reduced cladding surface heat transfer and as the system pressure drops below the fuel rod internal pressure, the zircaloy cladding may balloon and rupture. Significant cladding oxidation will occur at temperatures above about 1100 K. At cladding temperatures above 2250 K, the oxygen-stabilized alpha zircaloy will melt and possibly dissolve a significant amount of UO_2 . Resolidification of the liquified fuel rod material in the lower portion of the test bundle or core could cause extensive blockages of coolant subchannels. Quenching of the oxidized and embrittled cladding will probably result in fragmentation of the fuel rods, thus creating a large rubble bed composed primarily of slag (previously molten material) and fragmented ZrO_2 and UO_2 . Fission products will be released to the system when the cladding balloons and ruptures. Additional fission product release can occur from dissolution of UO_2 and also from pellet fragmentation and desintering.

The time required for a small break LOCA is much longer than for a large break LOCA, in which depressurization of the system is usually completed within approximately 35 to 40 s. The coolant thermal hydraulics and the heat transfer from the fuel to coolant are complex, involving long periods of convection cooling, boiloff of the coolant, convection and radiation heat transfer in the dry region, and, finally, a return to convection cooling as the core is reflooded and quenched. Due to the long periods of time at high temperature in a steam atmosphere, zircaloy cladding ballooning, rupture, oxidation, and embrittlement are all important phenomena in determining the thermal and mechanical response of the fuel rods.

3. OBJECTIVES OF THE SUPER-SARA SMALL BREAK LOCA TESTS

Because of the many possible small break LOCA scenarios, the SUPER-SARA Test Program¹ is directed toward providing data that will characterize the primary modes of fuel rod behavior summarized in Section 2.

The principle areas of interest include

1. Cladding ballooning and rupture (at low heating rates with minimal axial and circumferential temperature differences).
2. Cladding oxidation and embrittlement.
3. Fuel rod fragmentation when the core is quenched (cladding and fuel fracture and fuel desintering).
4. Fuel dissolution by molten cladding at temperatures above 2250 K, and the redistribution and solidification of this molten material. Blockage of coolant flow channels within the test bundle could be extensive, which in turn could severely restrict the long-term coolability of the rubble pile.

Four types of tests are currently planned to systematically evaluate the fuel bundle response at temperatures ranging from 1700 to 2300 K. The four types of tests are summarized as follows from Reference 2.^a

Type 1 - Tests involving cladding ballooning and rupture without prior cladding oxidation. The test conditions would include $\Delta P > 0$ ^b, and maximum cladding temperatures in the range 1100 to 1200 K.

a. These are the types of tests proposed by the ESSOR staff. EG&G Idaho feels that the program should emphasize high temperature tests and the effects of heating rate.

b. ΔP = pressure differential across the fuel rod cladding between the rod internal pressure and system pressure, i.e., $\Delta P = P_{int} - P_{system}$.

- Type 2 - Tests involving cladding oxidation, but no cladding ballooning. Test conditions would include $\Delta P < 0$, with no constraint on maximum cladding temperature.
- Type 3 - Tests involving cladding ballooning and rupture without prior oxidation, i.e., $\Delta P > 0$, with maximum cladding temperature ≤ 1200 K, followed by a continued temperature rise leading to external and internal cladding oxidation.
- Type 4 - Tests involving cladding ballooning and rupture with simultaneous and/or prior oxidation, and $\Delta P > 0$ with no constraint on maximum cladding temperature.

It is planned that the desired cladding temperature and rod pressure sequences necessary to attain these various types of fuel behavior will be accomplished by programmed reactor power, uncovering of the test bundle, and system pressure. Some of the tests will be terminated with a slow cooldown to preserve the bundle geometry for extensive posttest examination in the hot cell facilities. The remaining tests will be terminated with a quench to fragment the embrittled fuel rods and to evaluate the long-term (low coolant flow) cooling characteristics of the rubble pile.

4. SUPER-SARA TEST FACILITY

The SUPER-SARA facility is a high pressure water system capable of testing either single fuel rods or fuel rod clusters at both BWR or PWR pressures and temperatures. The main components of the once-through test section are the pressure vessel, the safety tube, and the instrumented test fuel rod cluster, shown in a side view in Figure 1. The pressure vessel is fabricated from zircaloy (2.5% Nb) for reasons of strength and neutron economy. It has an overall length of approximately 8.5 m, the internal diameter is 112.8 mm, the wall thickness is 11.5 mm, and it can accommodate up to 36 PWR fuel rods (6 x 6). Surrounding the pressure vessel is a safety tube which was designed and manufactured to the same standards as the pressure vessel. The safety tube is approximately 7.6 m long by 149 mm in internal diameter, with an 8.1-mm wall thickness. It covers the pressure vessel over its in-pile length and provides an annular gap around the primary containment.

The fuel bundle for the small break test program will consist of 36, zircaloy clad, UO₂ fuel rods, arranged in a 6 x 6 square array within a zircaloy shroud, as shown in Figure 2. The fuel rods will be 2 m long and the fuel rod radial dimensions and spacing will be similar to a 17 x 17 PWR fuel element design. Table 1 summarizes the fuel rod characteristics.

TABLE 1. FUEL ROD CHARACTERISTICS

Number of rods	36
Rod outside diameter	9.5 mm
Diametral gap	0.1650 mm
Cladding thickness	0.572 mm
Cladding material	Zircaloy-4
Pellet length	13.46 m
Pellet diameter	8.16 mm
Pellet material	Sintered UO ₂

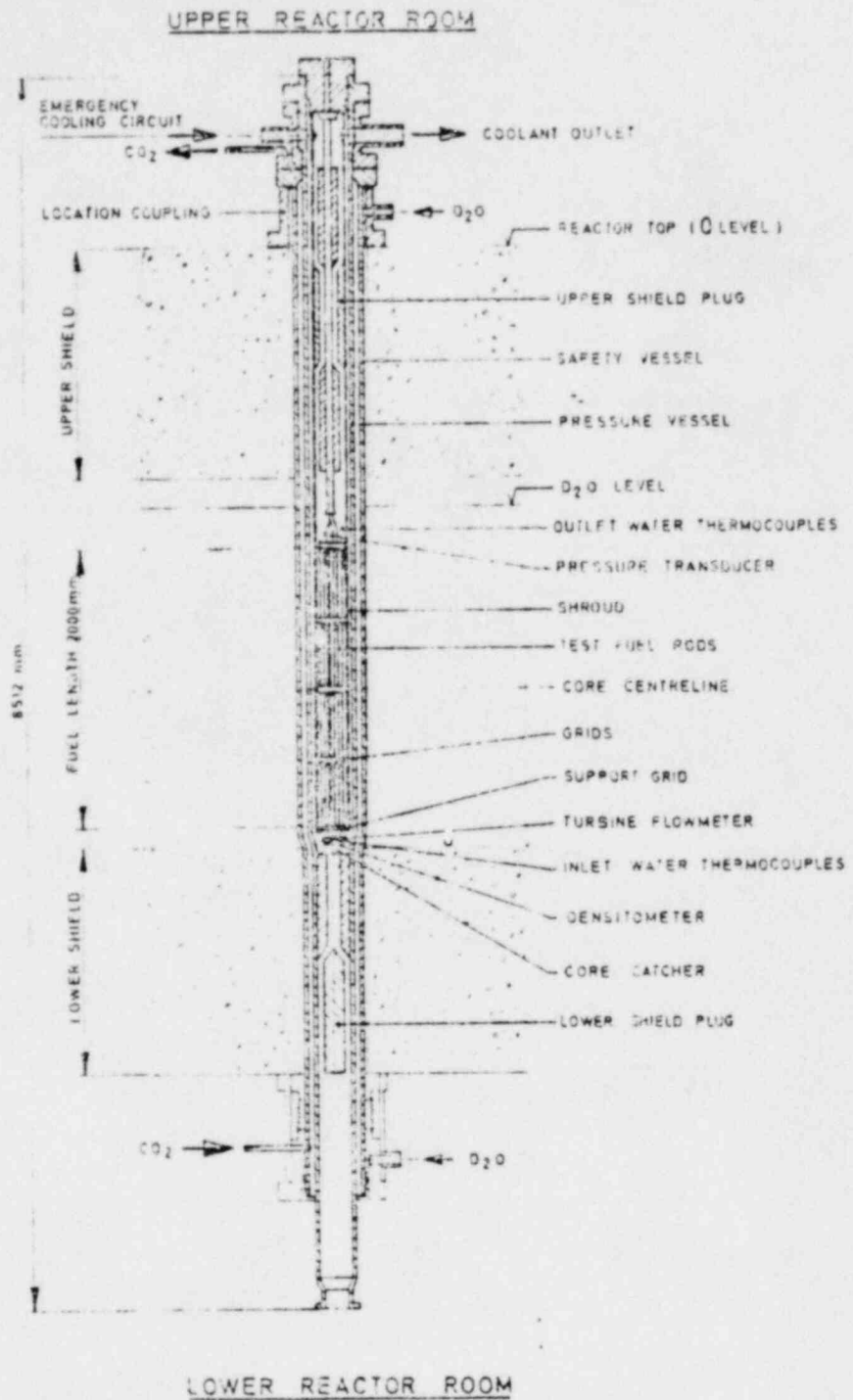


Figure 1. Vertical cross section of the SUPER-SARA in-pile test section (36 rods).

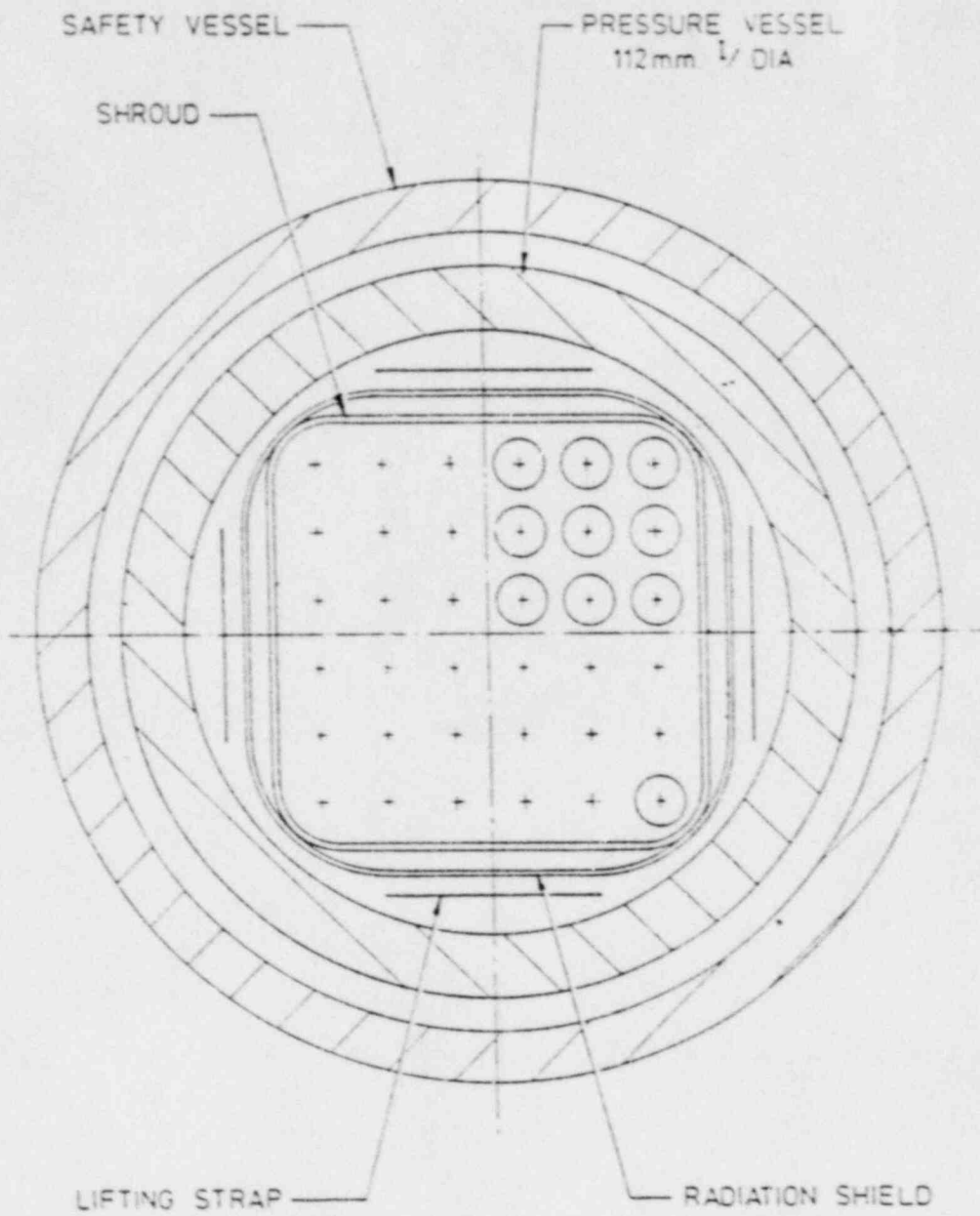


Figure 2. Horizontal cross section of SUPER-SAKA test section.

5. THE TRAC-BDO COMPUTER CODE AND MODEL FOR APPLICATION TO SUPER-SARA

EG&G Idaho is in the process of developing a capability for analysis of LOCA transients in BWR systems with the TRAC code. This computer model, TRAC-BDO, has been developed from TRAC-P1A⁴, the TRAC code for analysis of LOCA transients in PWR systems. The system conditions that will exist during the SUPER-SARA small break LOCA tests are appropriate for analysis with TRAC-BDO. A general description of some of the unique capabilities of TRAC-BDO that are applicable to small break LOCA analysis follows.

5.1 General Description of TRAC

The Transient Reactor Analysis Code (TRAC) is an advanced best-estimate systems code for analyzing accidents in LWRs. It is being developed at the Los Alamos Scientific Laboratory (LASL) and at the Idaho National Engineering Laboratory (INEL) under the sponsorship of the Reactor Safety Research Division of the U.S. Nuclear Regulatory Commission. TRAC-P1, completed in December 1977, was the first publicly released version and is described in the Los Alamos report LA-7279-MS. TRAC-P1 was designed primarily for the analysis of large break loss-of-coolant accidents (LOCAs) in pressurized water reactors (PWRs). TRAC-P1A is an improved version of TRAC-P1. While still treating the same class problems, TRAC-P1A is more efficient, and incorporates improved hydrodynamic and heat transfer models.

5.1.1 TRAC Characteristics

Some of the distinguishing characteristics of TRAC are summarized below. The state of the art in various areas is reflected in these capabilities.

A full, two-fluid, six-equation (mass, momentum, and energy), hydrodynamics approach is used to describe steam-water flow within a test bundle or core, thereby allowing such important phenomena as countercurrent flow and nonequilibrium thermodynamic effects to be treated explicitly. A full three-dimensional (r, θ, z) flow calculational capability exists;

however, for these calculations a one-dimensional fluid model was constructed. Since the interaction of the steam-water flow with the system structures is dependent on flow topology, the flow regime dependence of the constitutive equations has been incorporated into the model.

TRAC incorporates a detailed heat transfer analysis capability that includes a reflood tracking capability for both bottom flood and falling film quench fronts. The heat transfer from the fuel rods and other system structures is calculated using flow regime dependent heat transfer coefficients obtained from a generalized boiling curve based on local coolant conditions.

An important feature of TRAC is the ability to address entire accident sequences, including computation of initial conditions, with a consistent and continuous calculation. For example, the code models the blowdown, heatup, and reflood phases of a LOCA. This eliminates the necessity of synthesizing several calculations performed with different codes to complete the analysis of a given accident.

5.1.2 Physical Phenomena Treated

Because of the detailed modeling in TRAC, much of the physical phenomena important in small break LOCA analysis can be treated. Included are counter current flow, bottom reflood and quench, liquid entrainment during uncovering of the core due to boiling and during reflood, phase separation, and zircaloy metal-water reaction.

5.2 Description of TRAC-BDO Code

TRAC-BDO is a preliminary version of TRAC developed at the INEL for analysis of LOCAs in boiling water reactors (BWRs). In addition to accounting for geometric differences between BWRs and PWRs, TRAC-BDO takes into consideration the important influence of radiation heat transfer to the fuel canister walls when the bundle is steam filled.

An important new component called CHAN (for channel) has been developed to enable realistic and detailed modeling of the test bundle fuel rod heat transfer and thermal hydraulics. The heat transfer modes provided for the CHAN calculation include:

1. Conduction heat transfer in the fuel rods and the channel wall.
2. Convective heat transfer from the fuel rods and channel wall.
3. Radiation heat transfer from rod to rod, rods to shroud, rods to steam, and rods to water droplets.

Existing TRAC-PIA models are used for the conductive and convective heat transfer modes. A diffuse gray body model with steam and droplet participation was developed for the radiation heat transfer model. This model is similar to the models used in the NORCOOL⁵ and MOXY-SCORE⁶ codes. The major differences between the TRAC-BDO radiation model and the NORCOOL and MOXY-SCORE models are in the methods of calculating emissivities and absorptivities of steam and water droplets.

The one-dimensional model for the rod bundle hydrodynamics analysis is a drift-flux model involving the steam-water mixture velocity and the relative velocity between phases. The relative phase velocity is calculated from the Zuber-Findlay⁷ or Ishii⁸ correlations, depending on the specific flow regime.

The specific variables calculated and provided as printout by TRAC-BDO, along with the identifiers and units for each variable, are described in Appendix A.

5.3 TRAC-BDO MODEL FOR SUPER-SARA

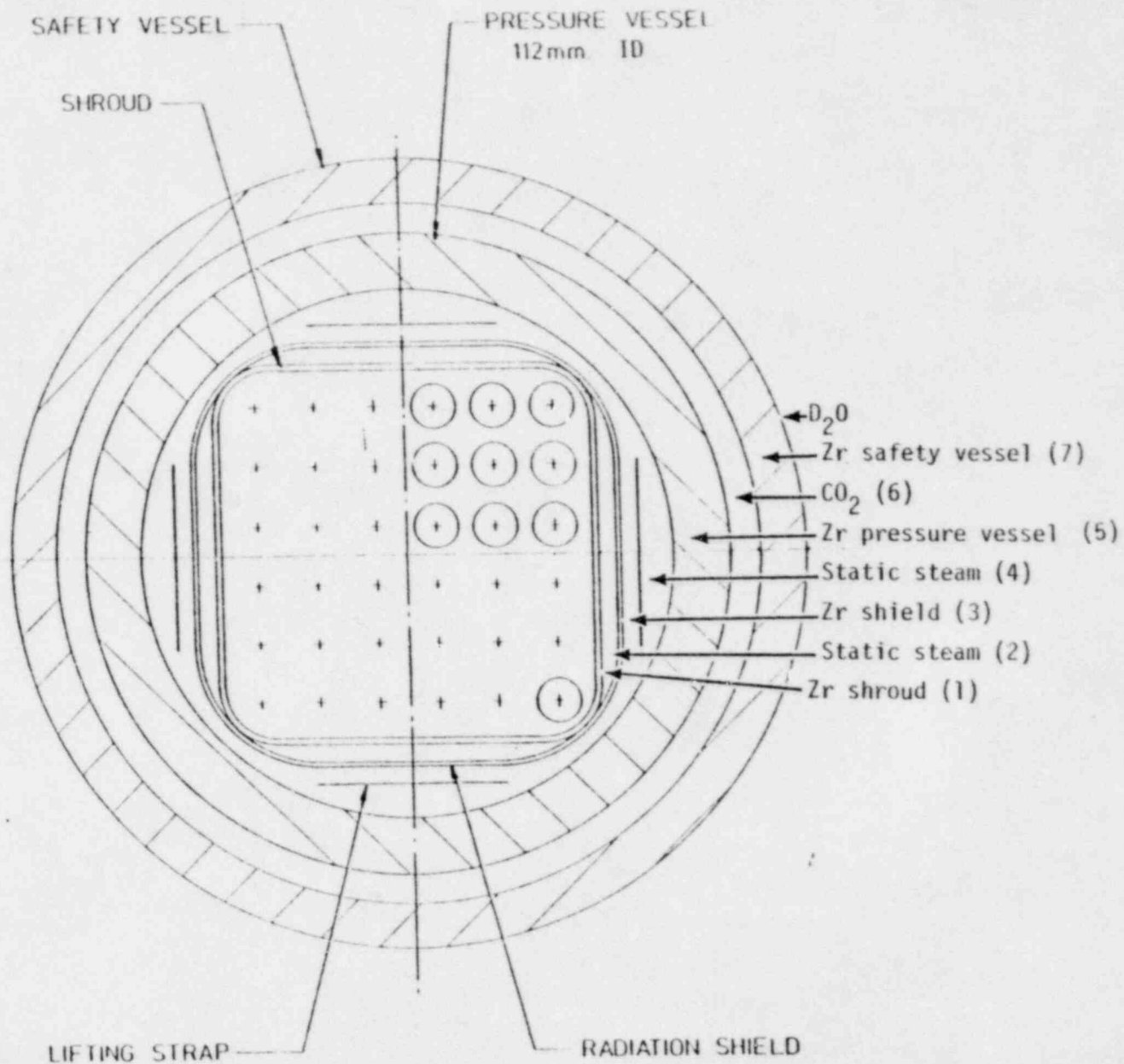
The proposed SUPER-SARA tests are modeled such that a single TRAC-BDO CHAN component represents the 36-rod cluster, flow shroud, and pressure vessel. The calculation is performed by specifying the necessary

thermal-hydraulic boundary conditions, such as inlet coolant flow rate, temperature, pressure, test rod power densities, and pressure vessel outside wall temperature.

A cross-sectional view of the SUPER-SARA test rod cluster and associated regions and materials out to the safety vessel wall are shown in Figure 3. Surrounding the 6 x 6 rod cluster is a 1.2-mm-thick zircaloy shroud. Outside the zircaloy shroud is a region of static steam, 4.96 mm wide at the middle of the cluster and essentially zero thickness at the corners. This steam region is bounded by another 0.8-mm-thick zircaloy shield, which acts as a radiation shield. Between the radiation shield and the pressure vessel wall is an annulus of static steam. The pressure vessel is made of zircaloy (2.5% Nb) and is 11.50 mm thick. Between the pressure vessel and the safety vessel is a region of flowing CO₂, 24.7 mm wide. The safety vessel is also zircaloy (2.5% Nb) and is 8.1 mm thick. Outside the safety vessel is D₂O, the moderator-coolant for the ESSOR reactor.

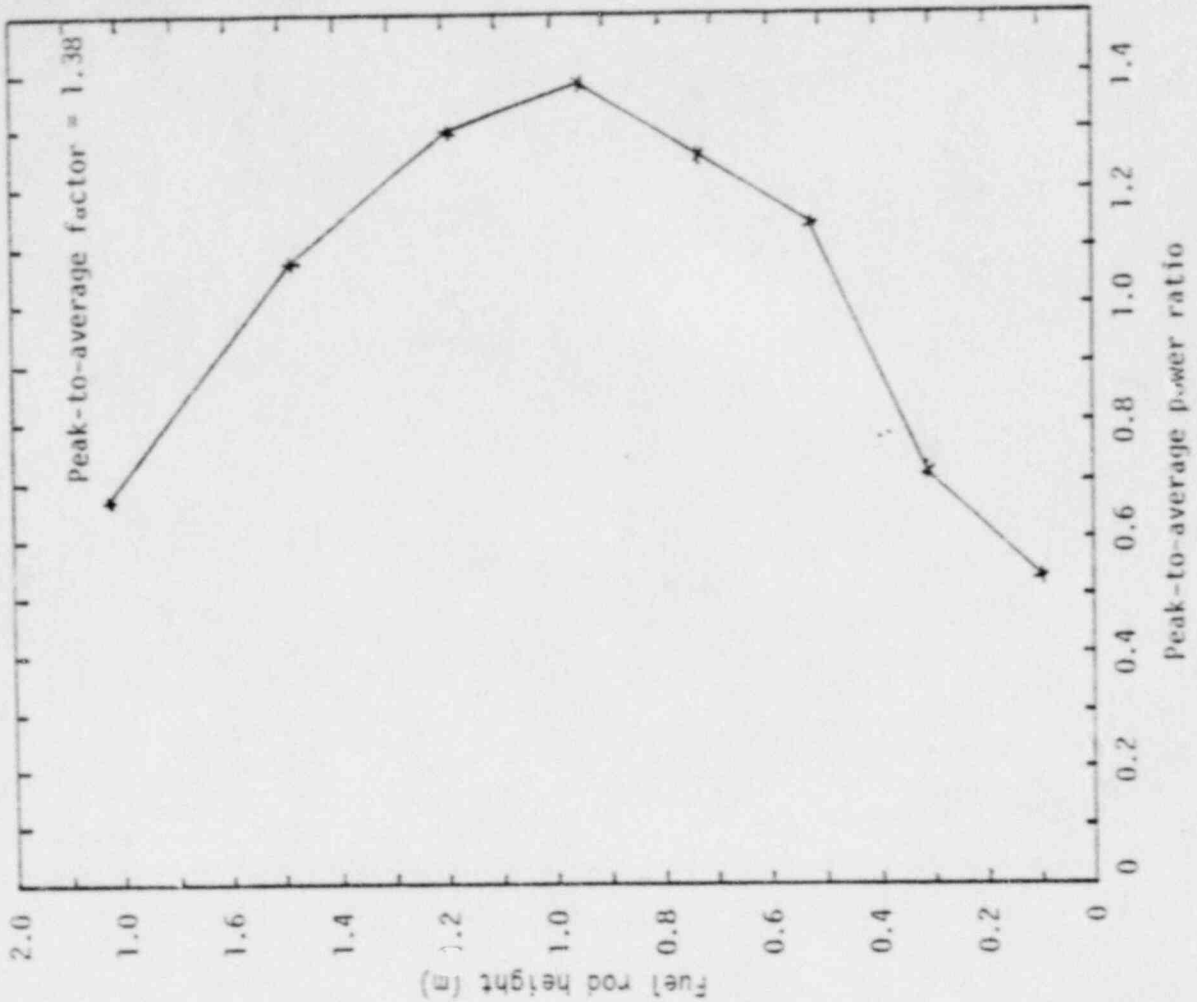
For purposes of calculating heat transfer through the various regions from the rod cluster to the outside of the safety vessel wall, an overall or lumped parameter heat transfer coefficient was calculated by the method described in Appendix B of this report.

The geometrical model used in TRAC-8DO is the same as shown in Figure 3, with the 2-m axial length of the fuel rods divided into 8 axial levels. At each axial level the power distribution across the cluster is assumed to be uniform. The dimensions of each axial level and the corresponding axial power distribution used in the model are shown in Figure 4. Symmetrical rods are grouped together at each axial level in Groups 1 through 6, as shown in Figure 5.



13

Figure 3. Horizontal cross section of SUPER-SARA test section showing the components modeled in TRAC.



8
7
6
5
4
3
2
1

Level	Height (m)
1	0.20955
2	0.20955
3	0.20955
4	0.20955
5	0.2380
6	0.2380
7	0.3429
8	0.3429

Figure 4. TRAC axial nodalization and the axial power distribution.

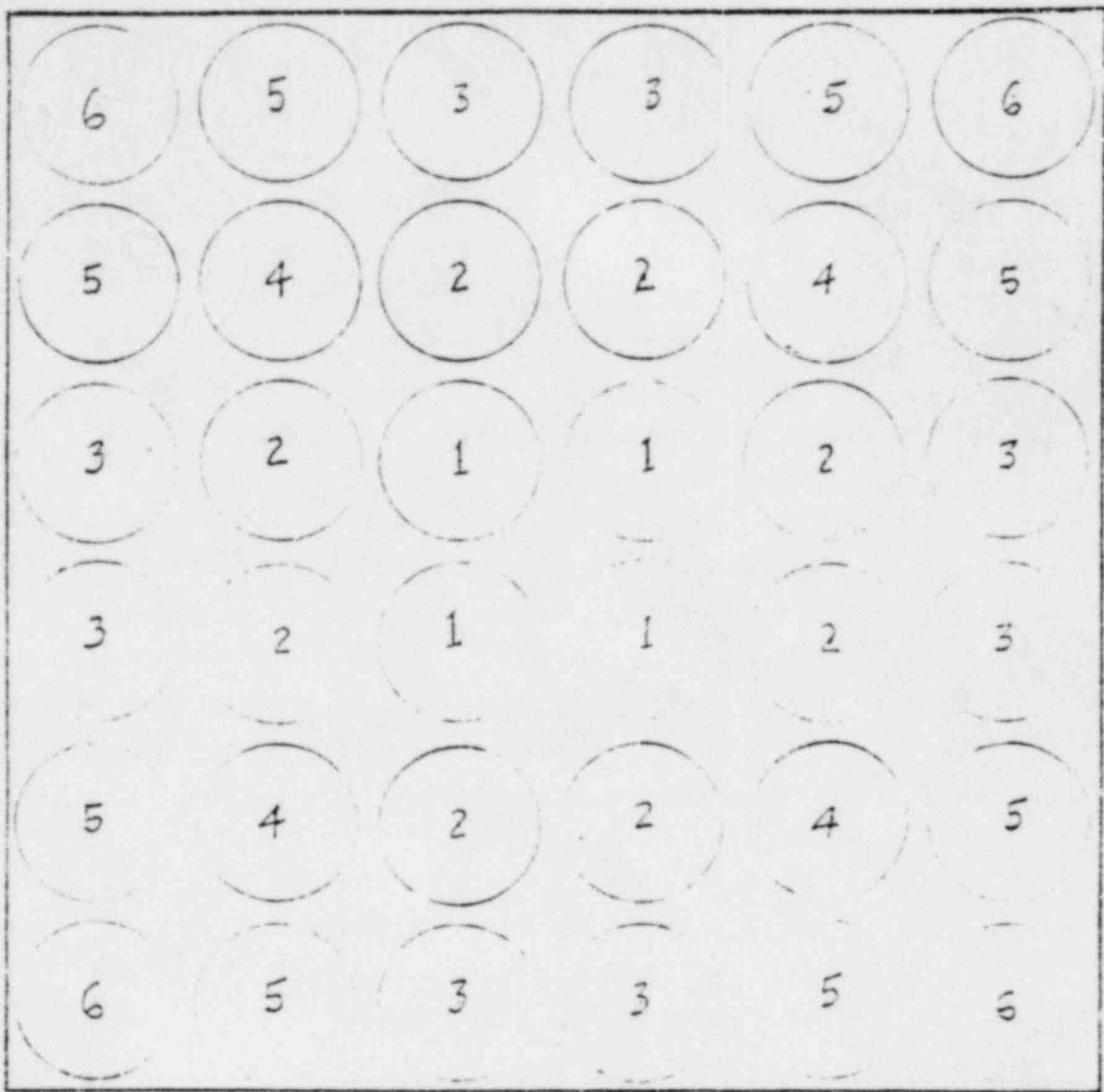


Figure 5. Fuel rod groups in the SUPER-SARA test bundle.

6. TRAC-BDO CALCULATIONS FOR SUPER-SARA SMALL BREAK LOCA TRANSIENTS

Two types of calculations were performed to evaluate the feasibility of performing small break LOCA tests in the SUPER-SARA test facility. For the first calculation, it was assumed that the coolant had boiled away to the extent that the rods were cooled only by steam at a low flow rate. The purpose of the TRAC-BDO calculations was to determine the equilibrium cladding temperatures as a function of steady state fuel rod linear power and steam mass flow, with the specific objective of identifying the conditions required to attain equilibrium cladding temperatures of approximately 1700 and 2300 K.

The second calculation better simulated a small break LOCA in that the coolant was assumed to have boiled down to approximately the axial midpoint (1 m level) of the test cluster. The objective of these calculations was to determine the test rod power and coolant mass flow rates required to attain equilibrium cladding temperatures of approximately 1700 and 2300 K, and to maintain the liquid level as close to the axial midpoint as possible.

The final calculated equilibrium conditions were of primary interest. Therefore, computer time and costs were reduced by initially selecting somewhat higher cladding surface temperatures than normal. This technique will provide correct equilibrium conditions; however, the system transient response may not be exactly representative.

The system conditions and the results of the calculations are described in Section 6.1 for the steam atmosphere test conditions and in Section 6.2 the steam/water test conditions.

6.1 Steam Atmosphere Test Conditions

Calculations were performed for the system thermal-hydraulic conditions of 7 MPa pressure and 559 K inlet steam temperature to determine the test rod peak power and steam mass flow required to obtain equilibrium

cladding peak temperatures of approximately 2300 and 1700 K. The calculated cladding peak temperatures, which occur above 1.66 m on the Group 1 rods, are shown in Figure 6. The calculated cladding peak temperature for a rod power of 3.61 kW/m and steam flow of 0.3 m/s was only carried out to about 800 s because it was apparent that the equilibrium temperatures would be significantly higher than 2300 K. A reduction in rod peak power to approximately 3.08 kW/m is shown to be adequate, at a steam mass flow rate of 0.0365 kg/s, to obtain a cladding peak temperature of 2400 K.

Calculated cladding peak temperatures are also shown, as the other three curves in Figure 6, as a function of increasing steam flow rate with the rod linear peak power held constant at about 3.08 kW/m. The cladding peak temperature is apparently quite sensitive to increased steam mass flow because of the influence of steam velocity on the surface heat transfer coefficient. Also, at the lower cladding temperatures the zircaloy-water reaction proceeds at a much slower rate, and thus there is significantly less energy generated by these rods, which also results in lower rod temperatures. A cladding peak temperature of approximately 1700 K can be obtained with a rod linear peak power of 3.08 kW/m by increasing the steam flow rate to 0.5 m/s.

Rod-to-rod temperature differences within the bundle for the two cases with cladding peak temperatures of approximately 2400 and 1700 K are shown in Figure 7. The predicted temperature differences from the center rod to the corner rod are only about 17 and 30 K, which is less than anticipated. The double-walled shroud with static steam voids and the pressure and safety vessels are treated as lumped parameter systems in the analysis, as illustrated in Appendix B. The primary resistance to heat transfer is the static steam voids, which are sandwiched between the zircaloy shrouds and the pressure vessel (Regions 2 and 4), and the flowing CO_2 (Region 6). This calculation is sufficient to indicate the relative heat transfer via convection to the steam and radial conduction across the shroud at stabilized conditions. At 1600 s, the ratio of convection to steam to radial conduction across the shroud is greater than 10:1. The one-dimensional formulation of the rod bundle hydrodynamics tends to

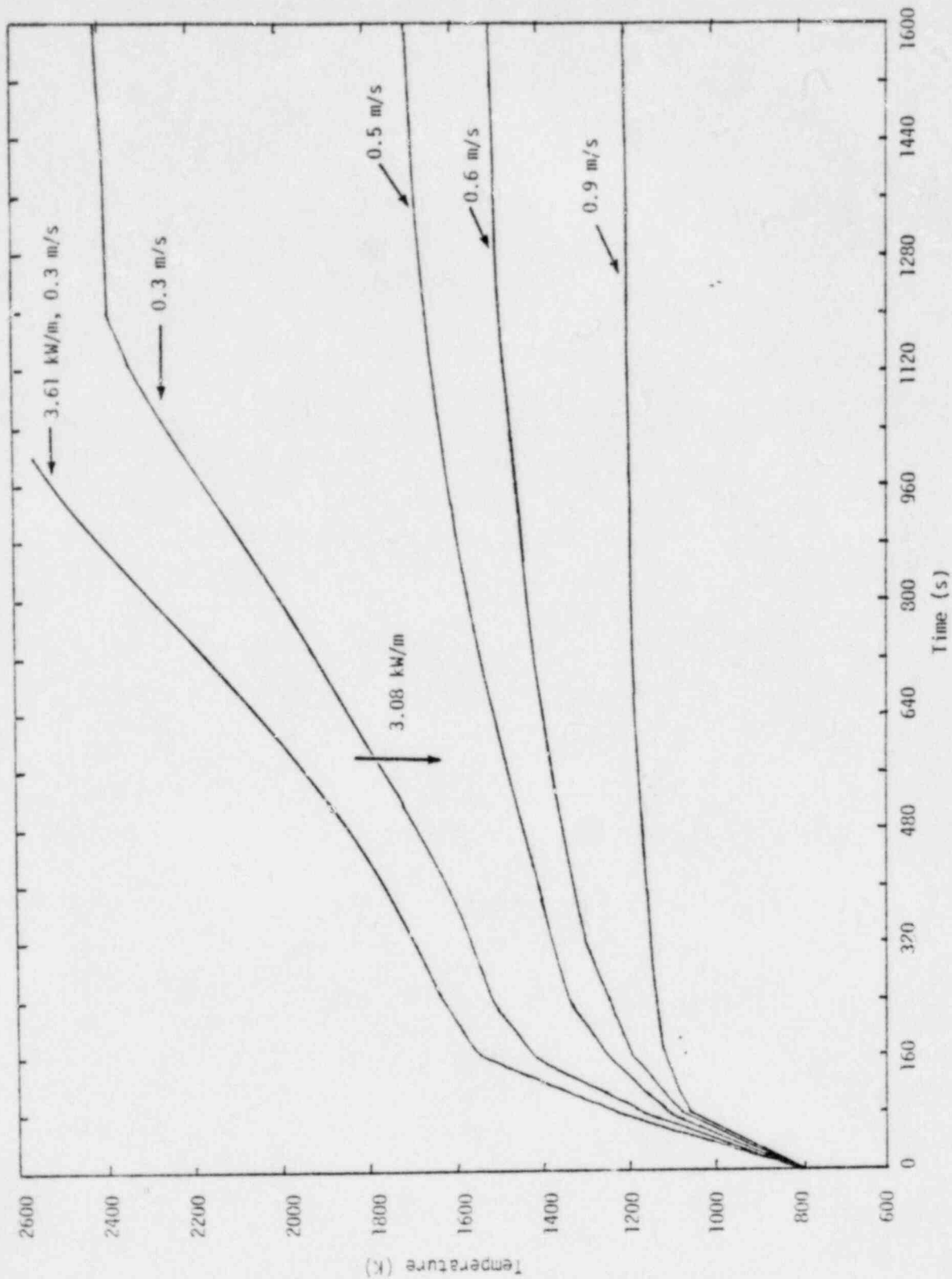


Figure 6. Map of calculated cladding peak temperatures as a function of linear peak power and steam flow rate.

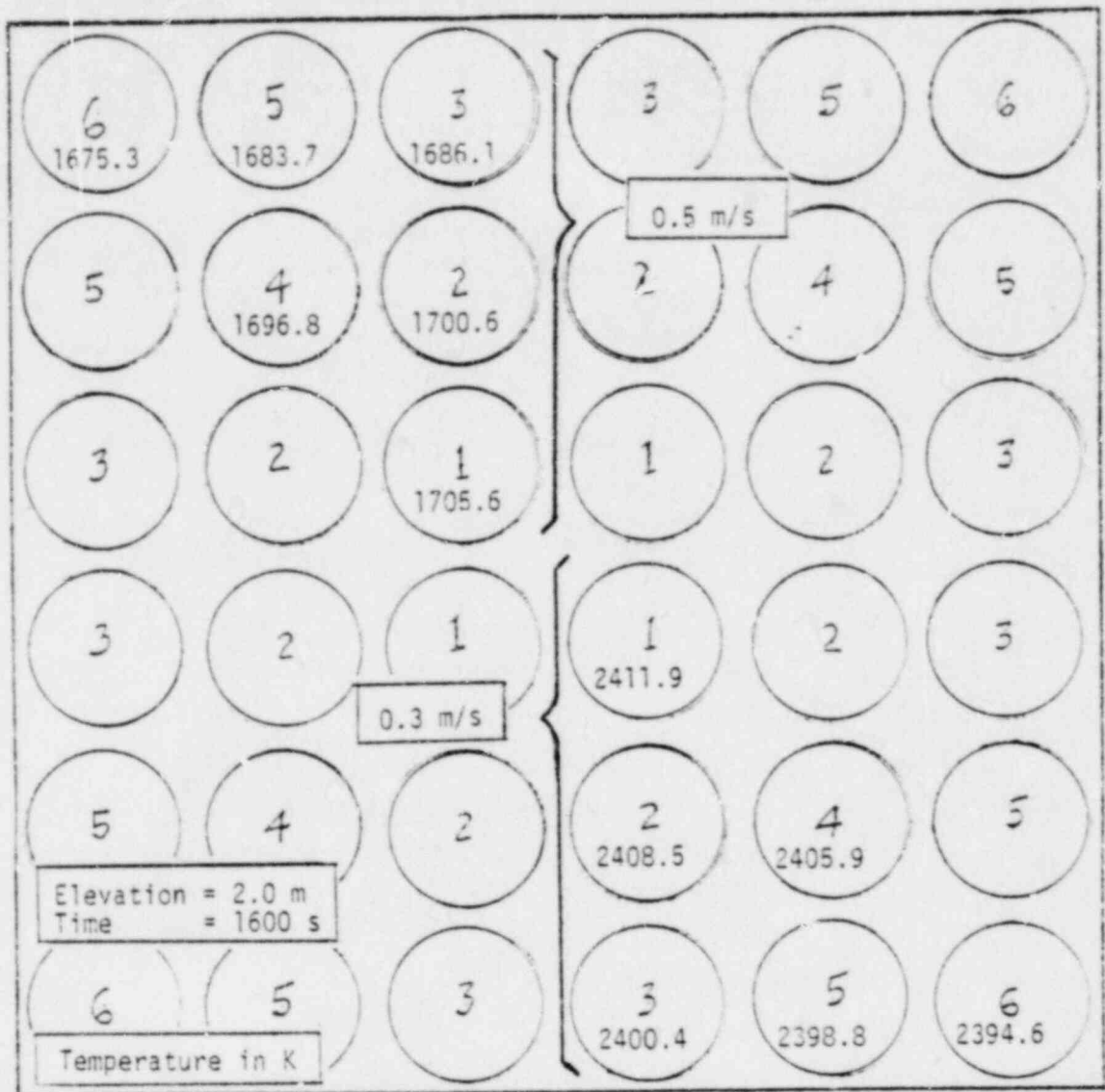


Figure 7. Calculated cladding peak temperatures in the SUPER-SARA test bundle at 0.31 kW/m linear peak power, and 0.3 and 0.5 m/s steam flow.

further minimize rod-to-rod radial temperature differences because it prevents temperature differences within the steam that would naturally develop from the bundle center to the shroud. The largest rod-to-rod radial temperature differences would occur prior to temperature stabilization because of the heat capacitance of the shroud. The CO₂ layer, Region 6, is the primary thermal resistance and the pressure vessel may require considerable energy to heatup as the system attains thermal equilibrium. However, this behavior cannot be evaluated with this analytical model.

In order to understand the thermal behavior of the bundle, it is necessary to examine the thermal response of the cladding, steam, and shroud inside surface; the metal-water reaction; and the modes of heat transfer as a function of both time at the high temperature elevation and elevation at 1600 s, (Figures 8 through 11). The calculated cladding peak, steam, and shroud inside surface temperatures as a function of time are shown in Figure 8. The cladding temperatures were initially less than the steam temperatures because of the method of initializing the calculation. With the steam flow at 0.3 m/s and the rod linear peak power at 3.08 kW/m, cladding temperatures rapidly increased because of the relatively low convective heat transfer to the steam. Steam temperatures then began increasing and, finally, the shroud wall temperature increased because of convective and radiative heat transfer from the steam and peripheral fuel rods, respectively, as shown in Figure 8.

Metal-water reaction became significant at about 100 s when the cladding temperature exceeded 1250 K (see Figures 8 and 9). The energy addition from the metal-water reaction caused the cladding temperatures to increase at a greater rate, which in turn increased the metal-water reaction. Gradually, an oxide layer developed and the metal-water reaction rate decreased. At approximately 1120 s, the zircaloy cladding was completely consumed and energy addition from the metal-water reaction was terminated. The end of the metal-water reaction correlates with the termination of the cladding temperature increase at about 1200 s,

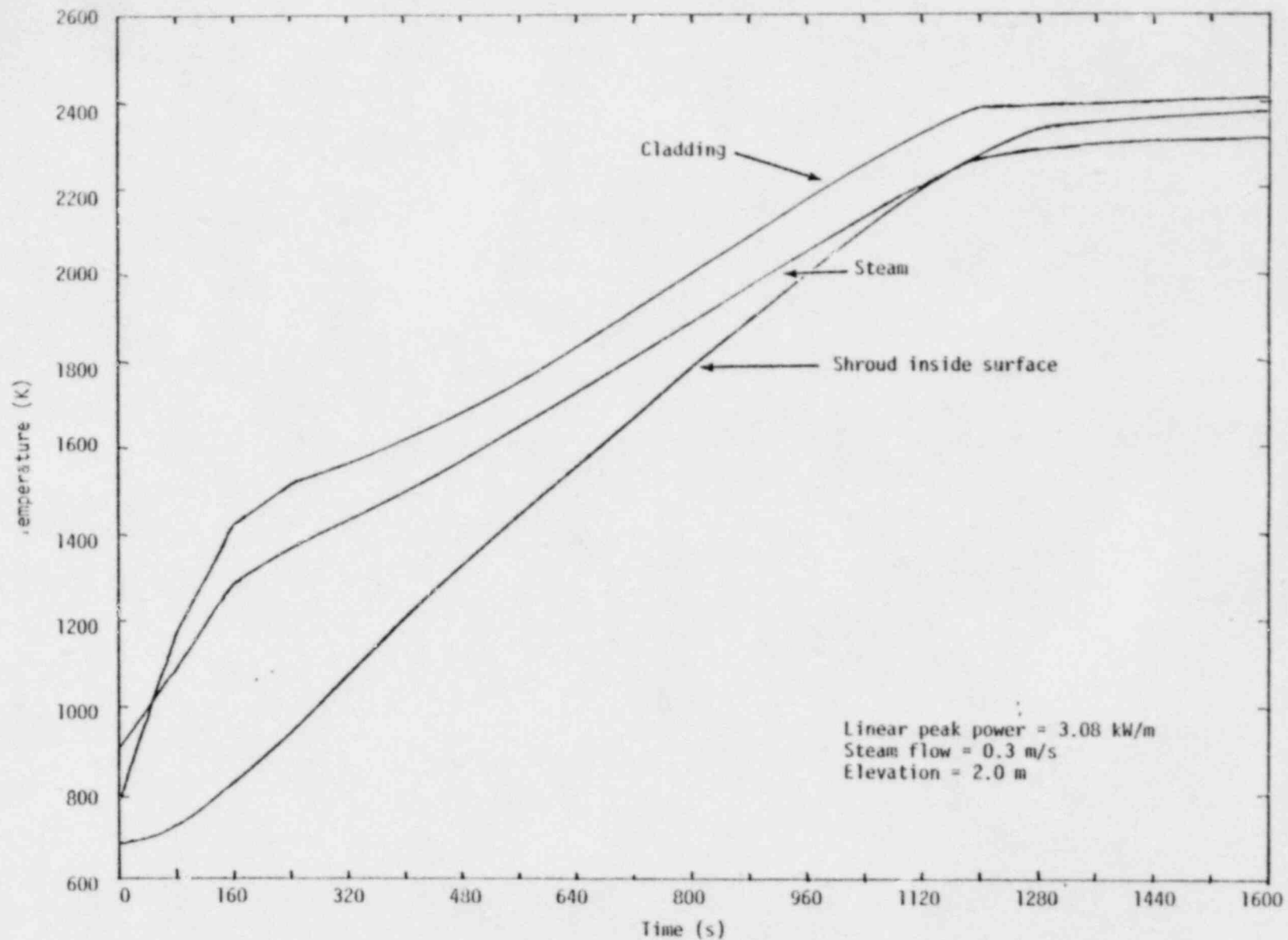


Figure 8. Cladding peak, steam, and shroud inside surface temperatures versus time for the calculation of high cladding temperature (~ 2400 K) with steam cooling.

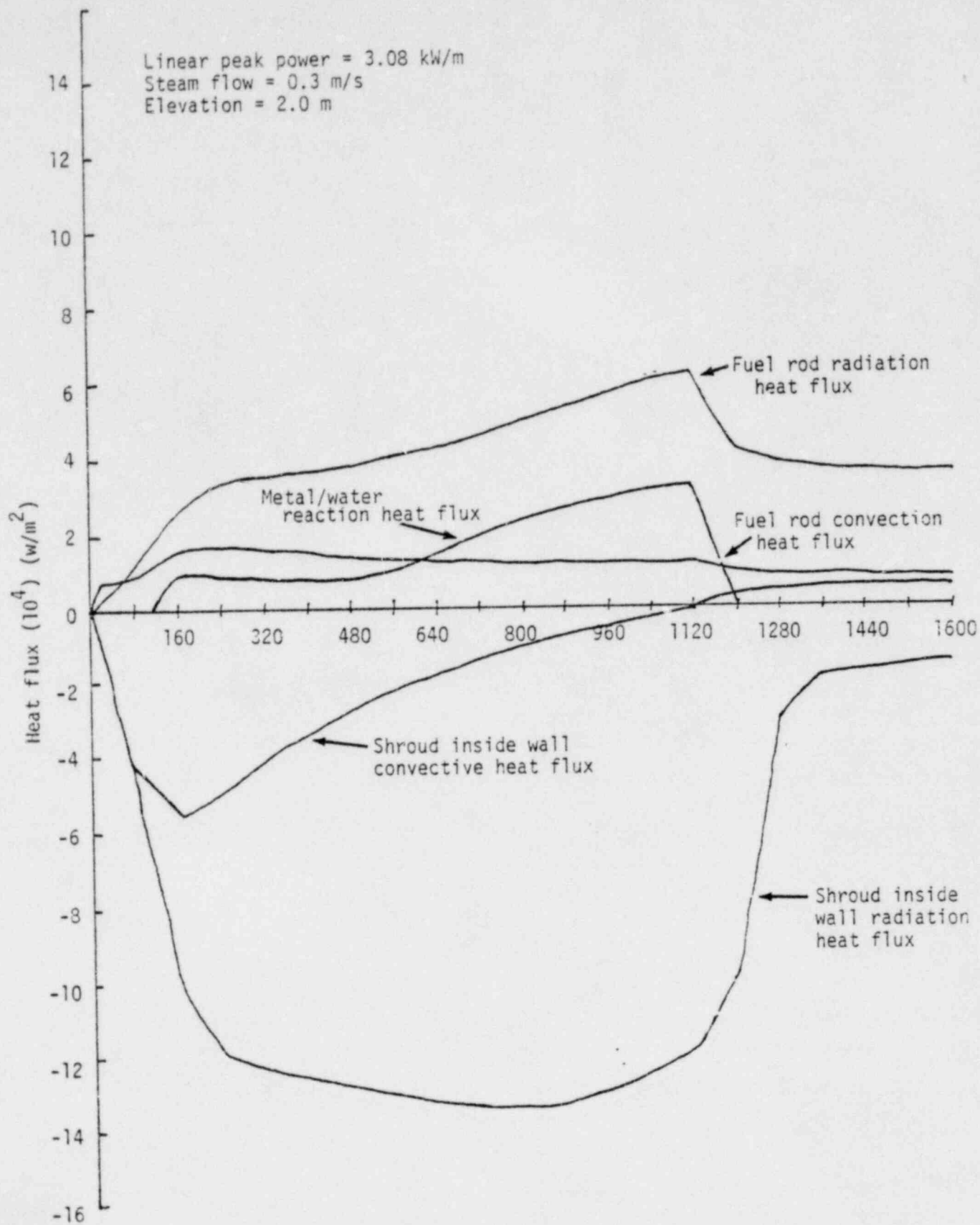


Figure 9. Fuel rod and shroud inside surface heat flux from the different heat transfer modes versus time for the calculation of high cladding temperature ($\sim 2400 \text{ K}$) with steam cooling.

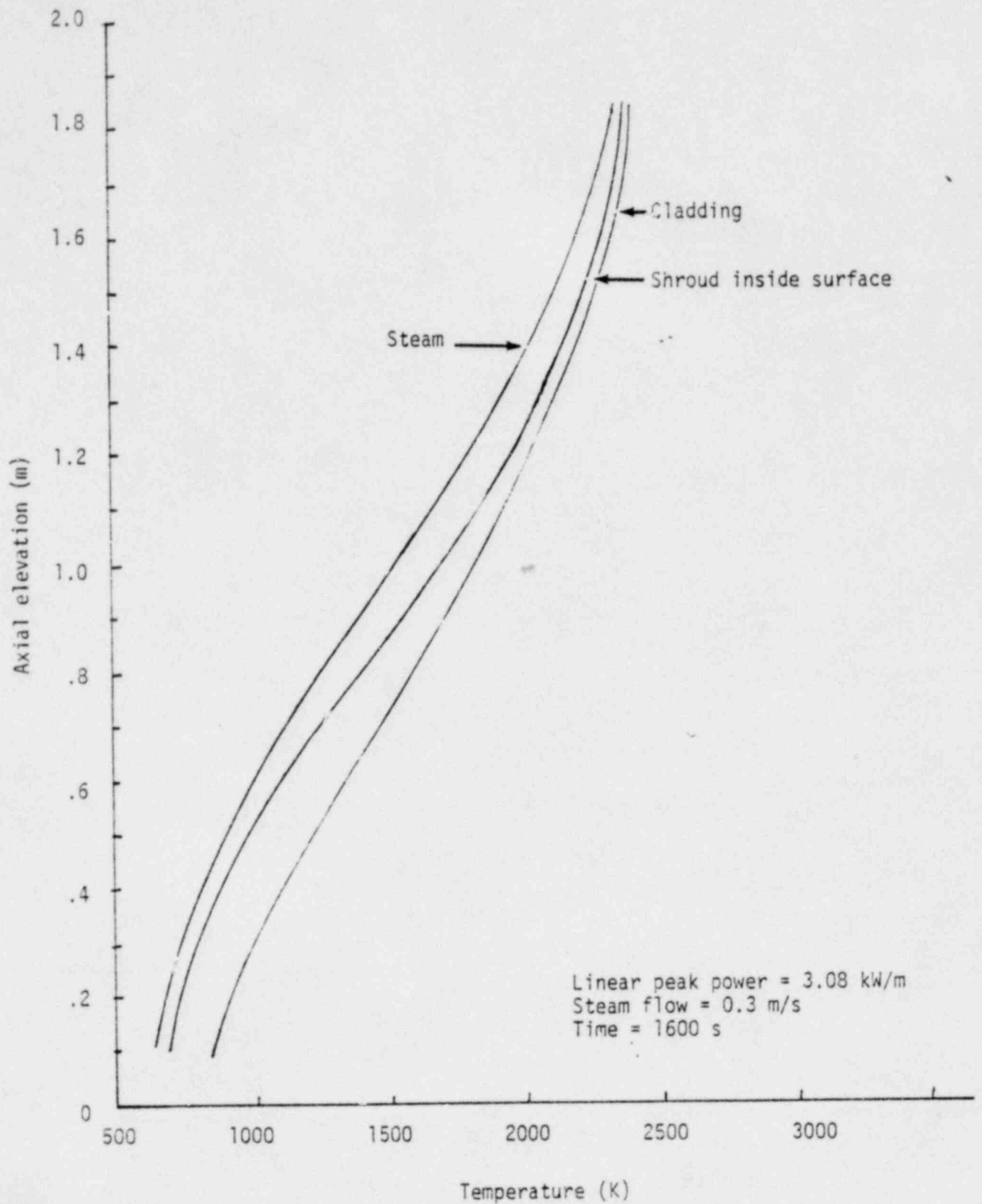


Figure 10. Cladding, steam, and shroud inside surface temperatures versus elevation for the calculation of high cladding temperature (~ 2400 K) with steam cooling.

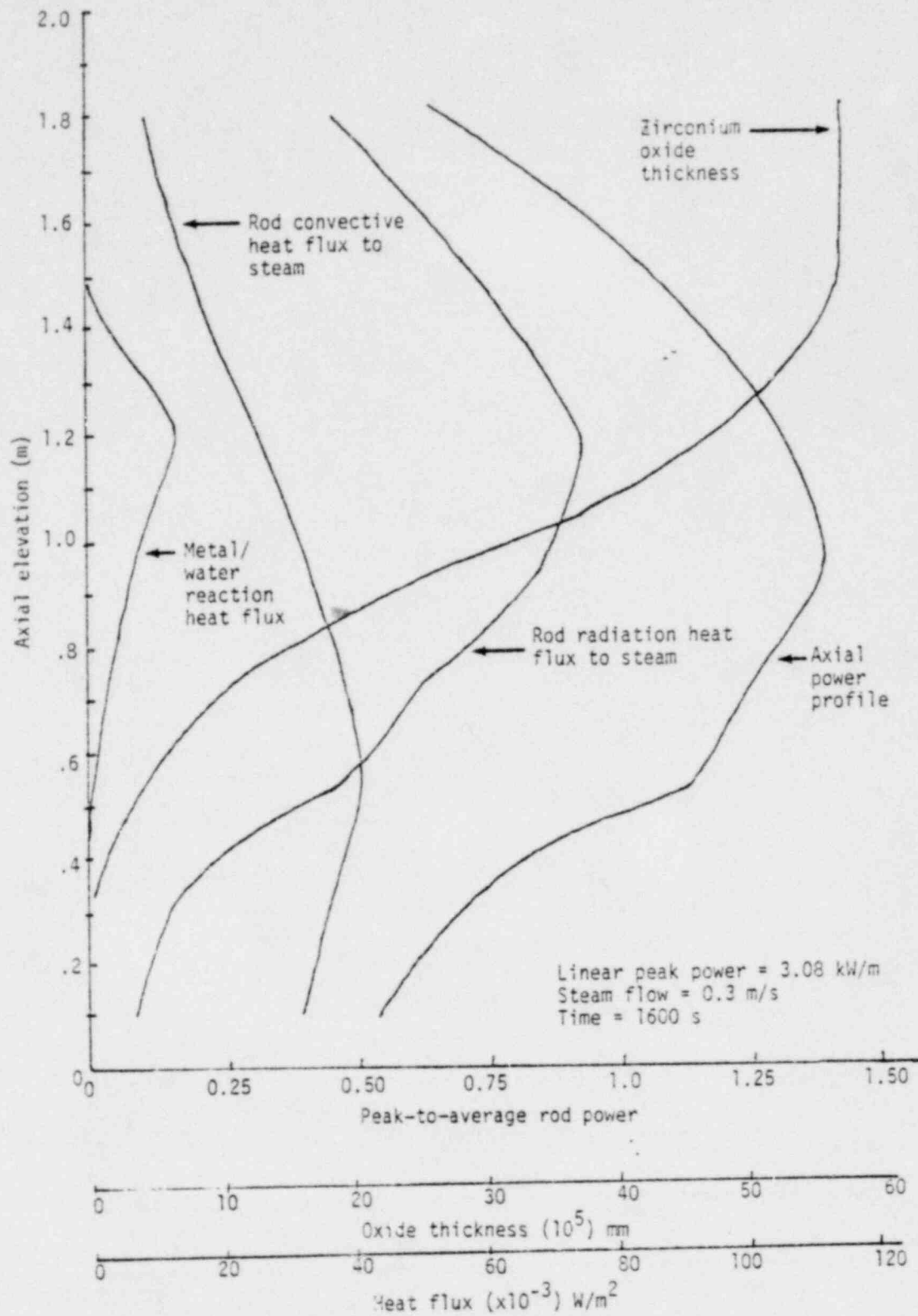


Figure 11. Rod surface heat flux, metal/water reaction heat flux, oxide thickness, and peak-to-average rod power versus axial elevation for the calculation of high cladding temperature (~ 2400 K) with steam cooling.

indicating that the cladding temperature increase was being driven primarily by energy from the metal-water reaction, and the stabilized temperature was maintained by fission heat.

The metal-water reaction did not completely consume the cladding at axial Level 8 between 1.66 and 2.0 m during the 1700-K case. Instead, it was predicted to be relatively constant from about 240 until 1600 s, thus permitting cladding temperatures to stabilize. When the metal-water reaction begins to decrease because of the developing oxide layers, the rod power will have to be increased to compensate for the reduced energy generation in order to maintain a constant cladding temperature.

When the cladding, steam, and shroud temperatures began to stabilize at about 1120 s, the stabilized shroud temperature was greater than the steam temperature. The relatively high radiative heat transfer from the peripheral fuel rods to the shroud resulted in greater heat transfer to the shroud than could be transferred radially by conduction. Therefore, the shroud inside surface temperature was greater than the vapor temperature in order to remove the heat from the system.

The axial profiles of cladding, steam, and shroud inside surface temperatures at 1600 s are shown in Figure 10. The same behavior, as discussed in the preceding paragraph, was predicted along the total axial length. The cladding peak temperature was predicted to occur at the top of the rod because the radial conduction through the composite shroud was insignificant compared with the convective heat transfer out of the bundle, and, therefore, system temperatures increased with elevation. To compensate for the decreased power generation with increased elevation, the cladding-vapor temperature difference decreased. The rate of change of cladding temperature as a function of increased elevation also decreased because of the reduced energy generation.

The rod convective and radiative surface heat fluxes, metal-water reaction, zirconium oxide layer thickness, and relative fuel rod power are plotted as a function of axial position at 1600 s in Figure 11. At the

bottom of the fuel rod, convection is the dominant mode of heat transfer because of the relatively low temperatures. Gradually, as temperatures increase with increasing elevation (see Figure 10), radiation heat transfer becomes significant at about 0.4 m and dominates above 0.6 m. The convective heat flux decreased above 0.5 m because the temperature difference between the cladding vapor was decreased. The fuel rod radiative heat flux is a maximum at 1.2 m, corresponding with the maximum in the combined energy generation by fission heat and metal-water reaction.

At 1600 s, the zircaloy metal-water reaction was predicted to be significant between about 0.5 and 1.5 m. Below 0.5 m, the cladding temperatures were less than 1250 K, too low for significant reaction. Above 1.5 m, the cladding was totally consumed by the oxidation reaction. The thermal conditions above 1.5 m were actually only in quasi-equilibrium because of the transient effects of the metal-water reaction between 0.5 and 1.5 m. The rate of change of the metal-water reaction was very slow at 1600 s because of the relatively thick oxide layer. However, as the reaction was slowly decreasing, cladding temperatures were also decreasing unless the rod powers were increased to compensate.

6.2 Steam/Water Test Conditions

Calculations were performed with the test cluster initially half full of water and system inlet pressure and temperature conditions of 7 MPa pressure and 576 K inlet coolant temperature, respectively. The objective of these calculations was to determine the combination of inlet coolant mass flow rate and minimum test rod peak power density that would provide rod peak cladding temperatures of approximately 1700 and 2300 K, and which also would maintain the liquid level as close to the initial 1-m axial position as possible.

Single-phase liquid coolant will enter the bundle at a low mass flow rate, vaporize while cooling the bundle, and exit the bundle as vapor when equilibrium is reached. The rod-to-coolant heat transfer processes within the bundle under these stabilized thermal-hydraulic conditions are shown

schematically in Figure 12. At the bottom of the bundle, heat transfer is by single-phase convection to the water. Nucleate boiling will commence when the water saturation temperature is reached, and then the heat transfer will change to forced convection boiling as the coolant quality increases and the flow regime changes from bubbly or slug to annular. Gradually, as the quality continues to increase, the fuel rod surface dries out and the heat transfer mode is dispersed-flow film boiling with radiation to the vapor and water droplets. The radiation component is not turned on in TRAC until the quality is at least 0.8. (This value is a user option.) When the quality is calculated to be 1.0, heat transfer is by forced convection and radiation to the steam. Between a quality of 0.96 and 1.0, the TRAC heat transfer routine linearly interpolates between the dispersed-flow film boiling and forced convection to vapor heat transfer modes.

A frothy mixture of flowing steam and entrained liquid will probably exist over a considerable axial length of the test bundle. For these conditions, it is not feasible to identify a distinct liquid/vapor interface. However, a "collapsed water level" can be defined, which is determined by calculating the amount of liquid present within each axial level, and artificially summing the liquid to an equivalent collapsed level. The formula that was used is

$$\text{Collapsed water level} = \sum_{i=1}^n (1 - \alpha_i) \frac{V_i}{A}$$

where

- α_i = vapor fraction in axial level, i
- n = number of axial levels
- V_i = volume of axial level, i
- A = cross-sectional flow area for each axial level.

The collapsed water level and the test rod cladding peak temperature are strong functions of the test rod peak power density and the coolant mass flow rate. The results from a parametric study to determine the effects of rod power density and coolant mass flow rate on test rod

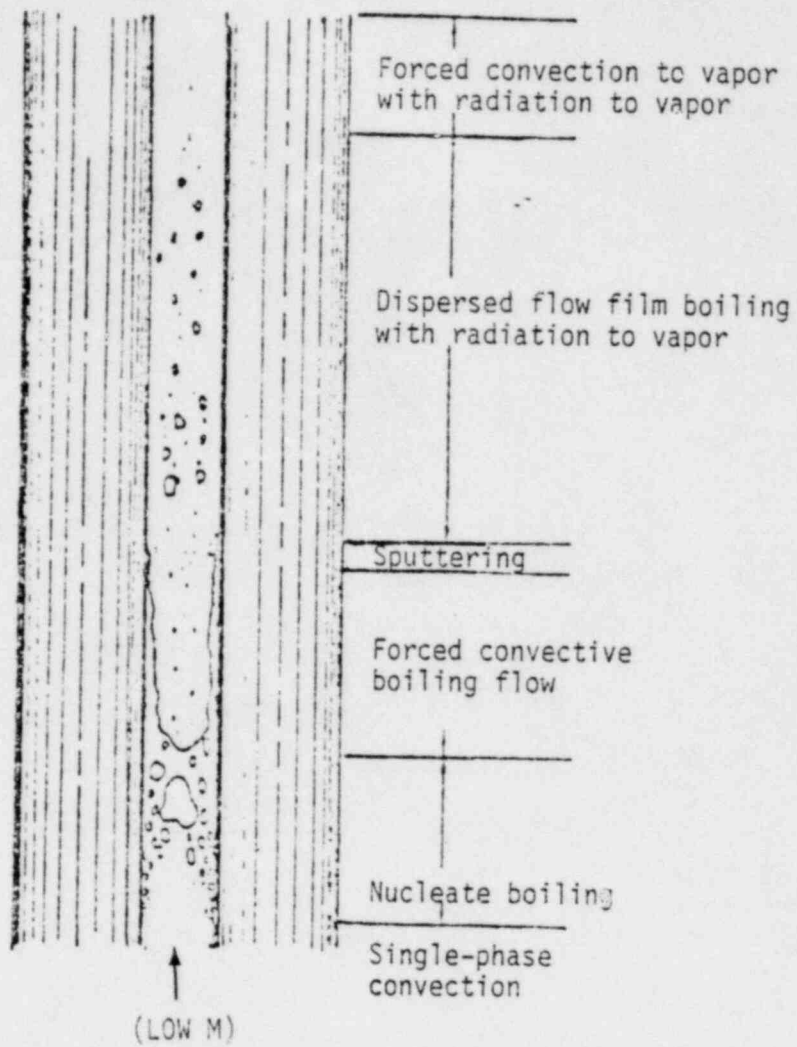


Figure 12. Heat transfer regimes modeled by TRAC-BDO at low inlet coolant flow.

cladding peak temperature and collapsed water level are shown in Figures 13 and 14. Test rod peak power densities were varied from 15.75 to 32.81 kW/m, and the coolant inlet mass flow rates were varied from 0.2 to 0.5 kg/s. The cladding peak temperature is shown to increase with increasing rod power and decrease with increasing coolant mass flow rate, as anticipated. A cladding peak temperature of 2300 K could be obtained with a linear peak power ranging from 22.64 to 32.81 kW/m and a coolant mass flow ranging from 0.2 to 0.3 kg/s.

The collapsed water level was predicted to increase with increasing coolant mass flow and decrease with increasing rod power, as shown in Figure 14. For the range of rod powers and coolant mass flow that will yield the desired cladding peak temperatures of 2300 and 1700 K, as illustrated in Figure 13, the collapsed water level will range from about 0.3 to 0.5 m. In other words, the range of the collapsed water level is only about one-half of that originally desired. Other calculations, not shown in Figure 14, were performed at linear peak powers greater than 32.8 kW/m and coolant mass flow rates in excess of 0.5 kg/s in an attempt to obtain the desired collapsed water level (~1.0 m) and cladding peak temperature (~2300 K). Cladding peak temperatures in excess of 1900 K could not be attained because coolant qualities were too low and the resultant dispersed-flow film boiling heat transfer coefficient was sufficient to keep cladding temperatures down. Of course, it would have been possible to further increase the fuel rod power and force the cladding peak temperature to increase, but this would have been inconsistent with the experimental objective of minimizing fuel rod power.

The rod-to-rod temperature distribution within the bundle for two cases with a linear peak power of 15.75 and 22.64 kW/m and a coolant mass flow of 0.2 kg/s is shown in Figure 17.^a The elevation of these

a. Although the predicted cladding peak temperature was 2200 K instead of the desired 2300 K, the calculation with a linear peak power of 22.64 kW/m and a flow rate of 0.2 kg/s was selected for detailed evaluation to illustrate the thermal characteristics of the bundle and fuel rods. Only a slight increase in the fuel rod power would be necessary to obtain a cladding peak temperature of 2300 K.

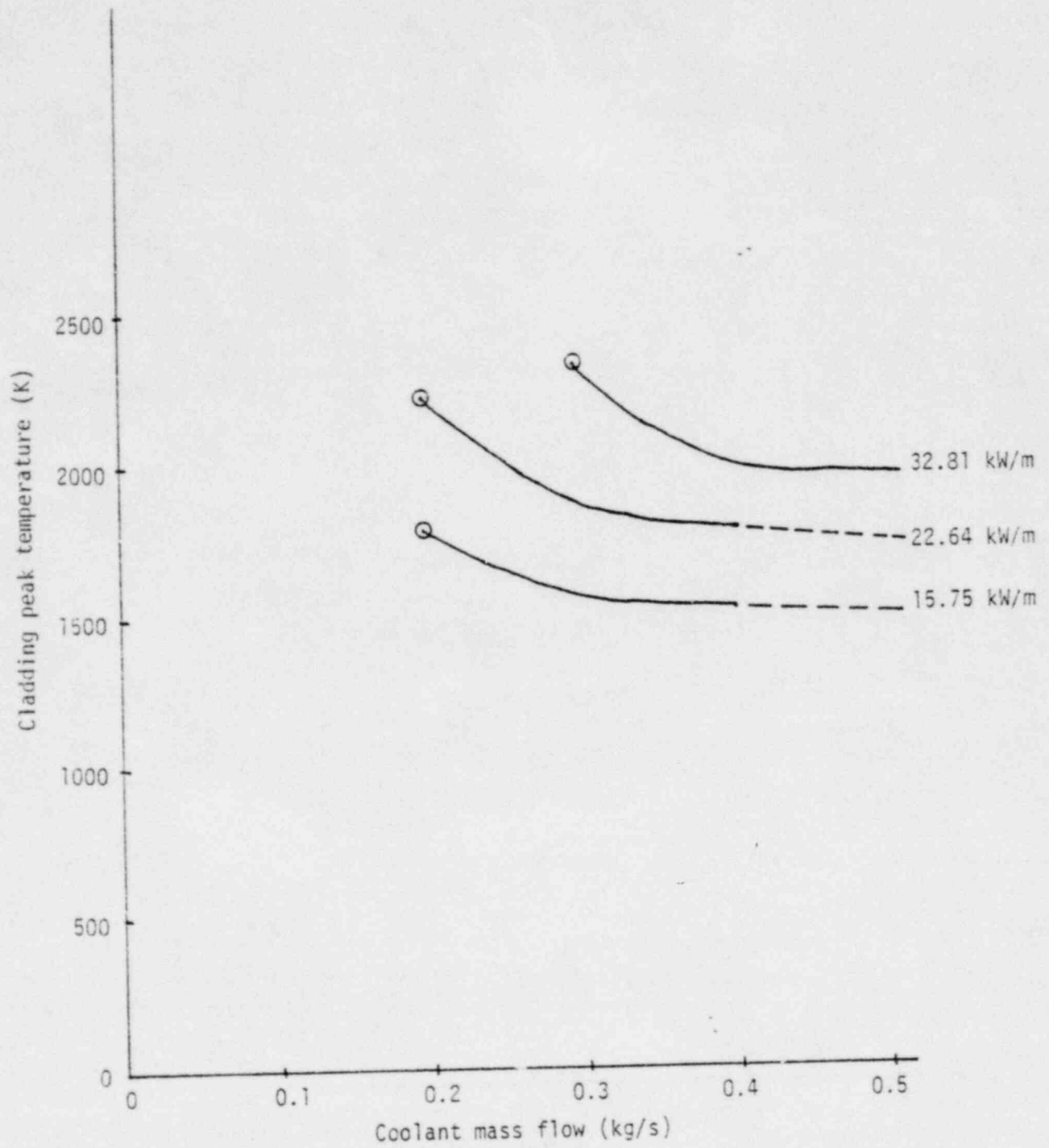


Figure 13. Calculated cladding peak temperatures as a function of both coolant mass flow and linear peak power for steam/water.

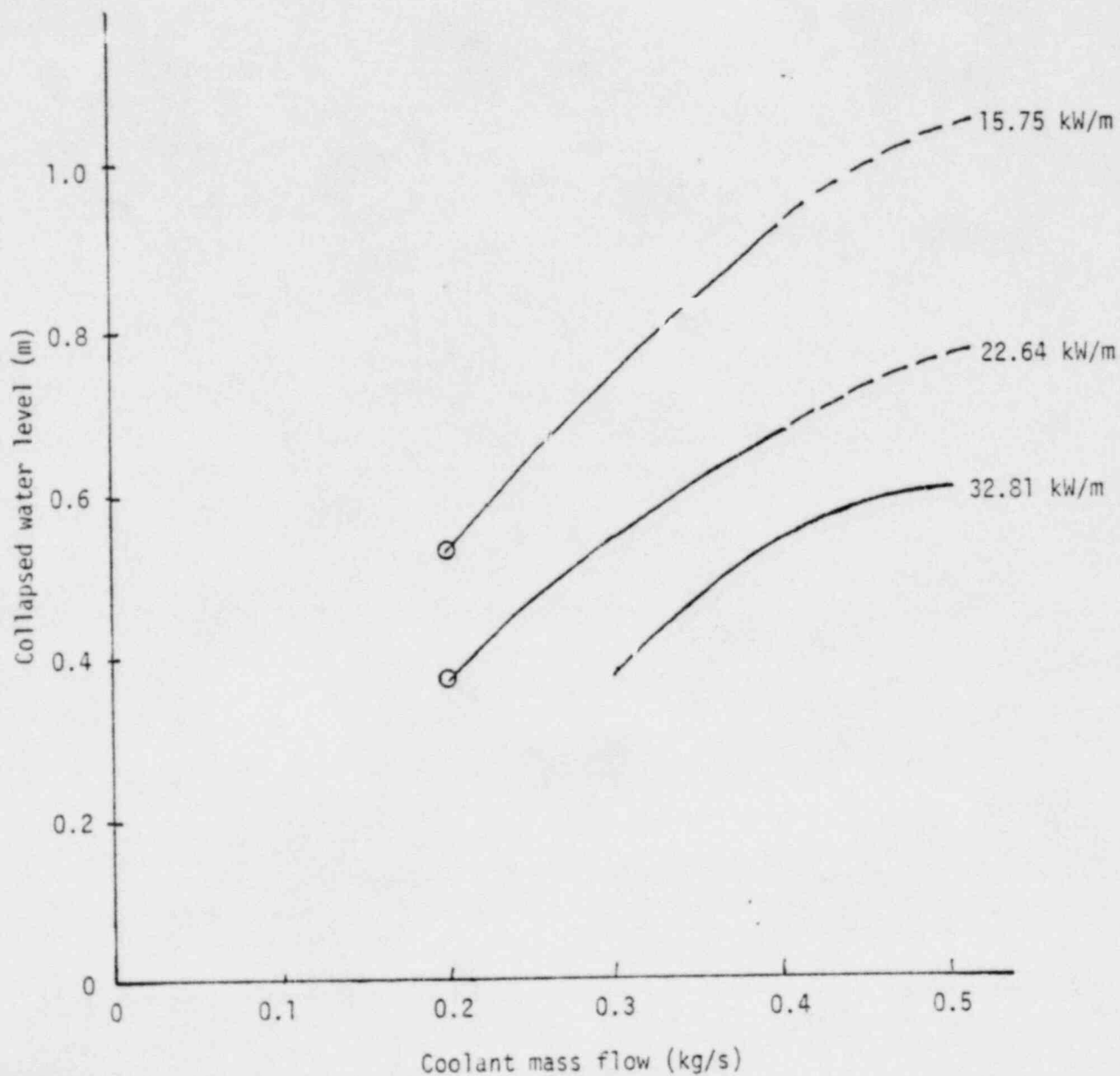


Figure 14. Map of collapsed water level within the bundle as a function of coolant mass flow and linear peak power.

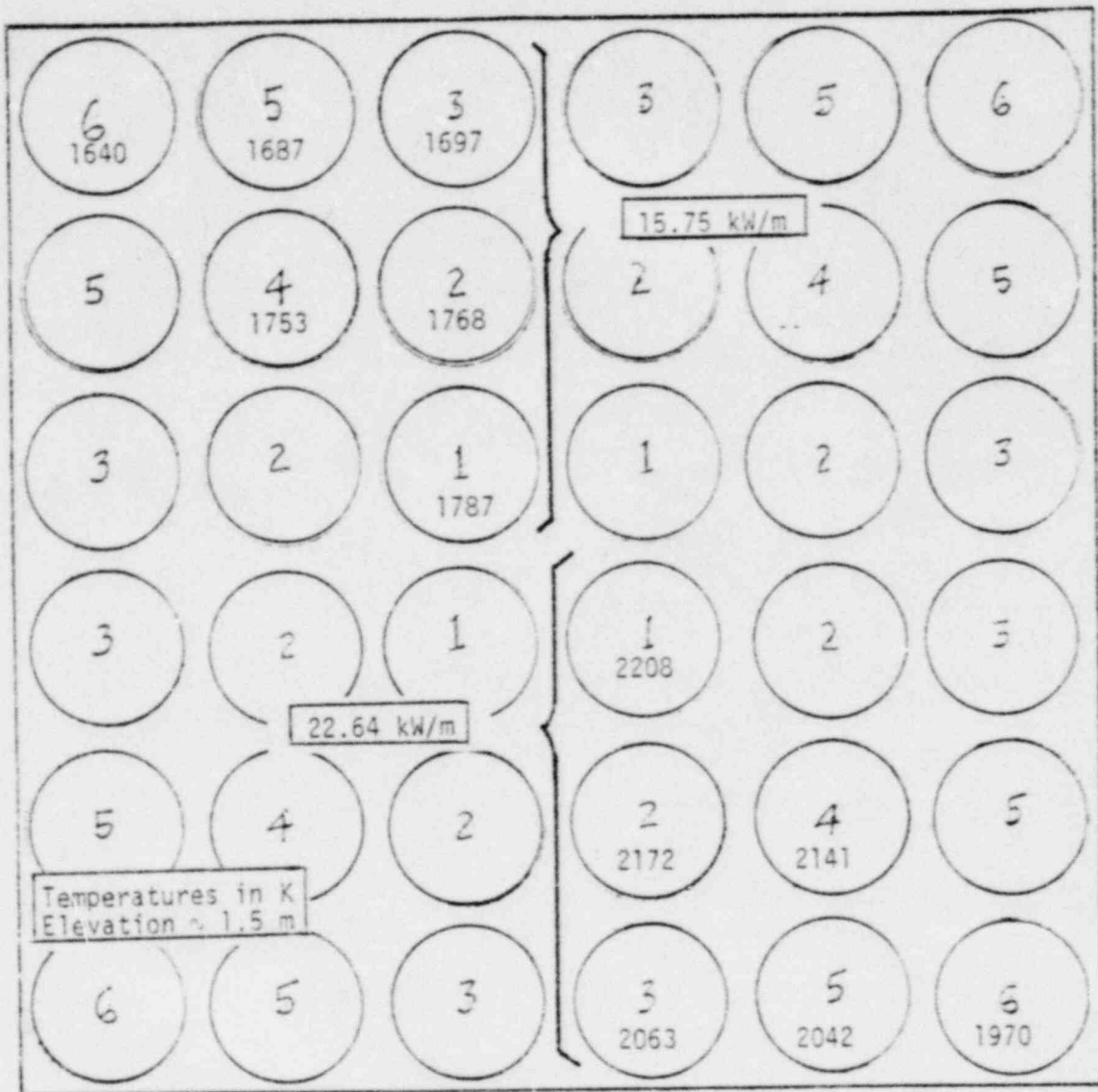


Figure 15. Calculated fuel rod peak temperatures in the SUPER-SARA test bundle at 15.75 and 22.64 kW/m, and 0.2 kg/s.

temperatures was approximately 1.5 m. The temperature difference from the innermost rod to the corner rod was approximately 150 and 240 K for the 15.75 and 22.64 kW/m cases, respectively. This temperature gradient across the bundle is significantly greater than calculated for an all-steam environment and is discussed in Section 6.1. The calculated wall temperature was only about 1000 K, with a resultant temperature difference between rods and shroud of about 1000 K versus only about 150 K for the calculation with all steam. The net result was that radiation heat transfer from the bundle peripheral rods was much more significant and provided some cooling. The shroud temperature was low at this elevation in the bundle because of substantial convective heat transfer to the steam.

The cladding peak temperature, steam temperature, and shroud inside surface temperatures for the 22.64 kW/m case are plotted as a function of time in Figure 16. The cladding peak temperature rapidly increased after the transient was initiated, and stabilized after only about 70 s. The relatively rapid stabilization of temperature occurred because of the high fission power generation. The metal-water reaction is not complete at 100 s and fuel rod power will have to be adjusted to compensate for changes in the metal-water reaction rate as the oxide layer develops in order to maintain a constant cladding temperature. The steam temperature has apparently stabilized, but the shroud temperature was predicted to still be slowly increasing. The increasing shroud temperature indicates that thermal equilibrium had not yet been reached when the calculation was terminated. However, significant increases in the cladding temperature because of the increasing shroud temperature would not be anticipated.

The heat transfer processes that occur during the transient at the elevation of the cladding peak temperature, ~1.5 m, are illustrated in Figure 17. Initially, the bundle was liquid filled to 1.0 m and, at the start of the calculation, violent boiling of the water occurred, generating a large volume of steam. As the steam rose through the bundle, it entrained liquid and carried the droplets to the top of the bundle. At the same time, the water volume within the bundle decreased and finally stabilized after about 60 s. At the high temperature elevation, ~1.5 m,

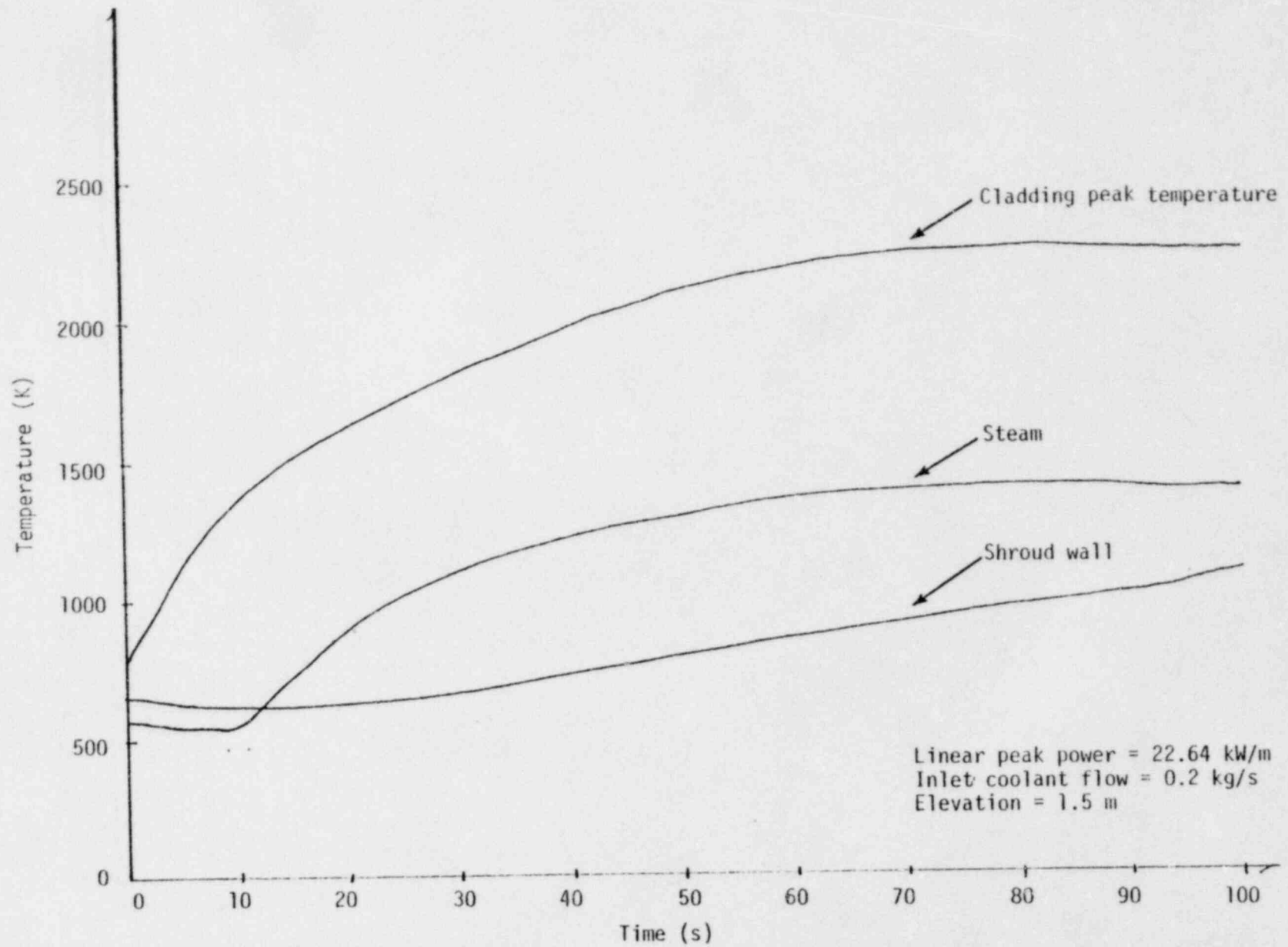


Figure 16. Calculated cladding peak, steam, and shroud inside surface temperatures versus time for the calculation of high cladding temperature with steam/water conditions.

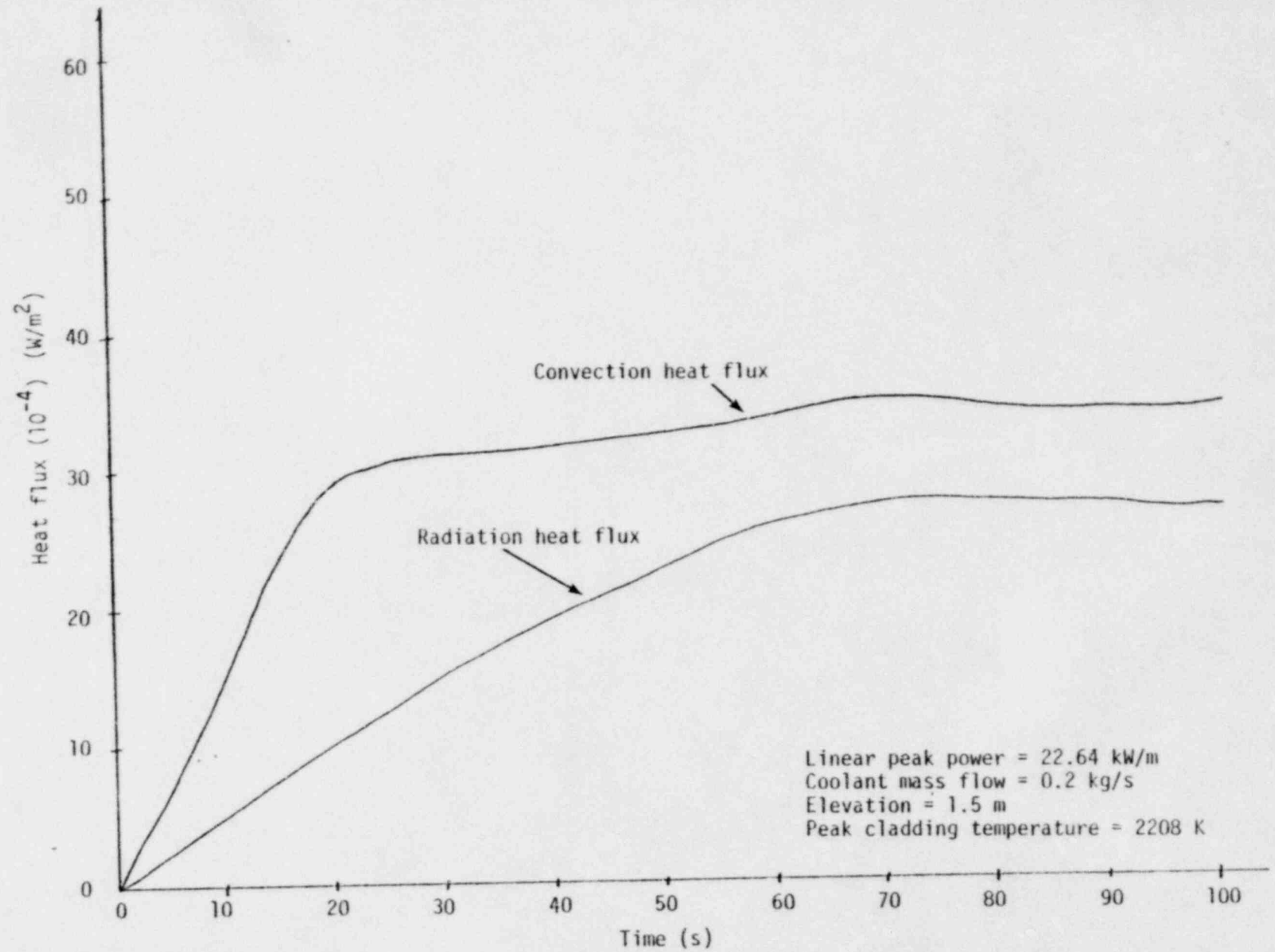


Figure 17. Fuel rod surface heat flux via convection and radiation versus time for the steam/water case at the peak cladding temperature elevation.

dispersed-flow film boiling was established almost immediately because of the entrained liquid and the relatively high initial cladding temperature. At about 5.0 s, the coolant quality reached 1.0 and the heat transfer mode changed to convection steam. Radiation to steam gradually became significant as cladding temperatures increased further.

The metal-water reaction heat flux and the oxide layer thickness are shown in Figure 18. The metal-water reaction was predicted to become significant at about 8 s when the cladding temperatures exceeded 1250 K. The reaction initially proceeded very rapidly because the initial cladding oxide thickness was small. However, at about 10 s the predicted cladding oxide thickness was sufficient to stabilize the reaction rate. At about 25 s the metal-water reaction rate again increased as a result of higher cladding temperatures. At about 55 s the metal-water reaction reached a maximum and decreased thereafter because the oxide layer tended to retard the reaction.

The fuel centerline, cladding surface, steam, and shroud inside surface axial temperature profiles at 100 s are plotted in Figure 19. Cladding temperatures were predicted to increase rapidly with axial elevation from about 0.1 m to the first maxima of approximately 2150 K, which occurred at about 0.5 m. Cladding temperatures then decreased to about 1800 K at about 0.85 m, and then increased again to the cladding peak temperature of 2208 K at about 1.5 m. Cladding temperatures again decreased from 1.5 m to the top of the fuel rod. The undulating cladding temperatures are not realistic, and are caused by discontinuities in the TRAC heat transfer subroutine during transitions between heat transfer modes. This code behavior will be discussed in the next paragraph. The decreasing fuel rod and shroud temperatures above 1.5 m also indicate that equilibrium conditions have not yet been established, although the rate of change of temperatures was quite slow (see Figure 15). As discussed in Section 6.1, the high thermal resistance of the shrouds and pressure vessel effectively limit radial conduction out of the bundle. Also, the coolant quality was essentially 1.0 above about 1.4 m, and steam temperatures could continually increase with elevation unless there is significant radial

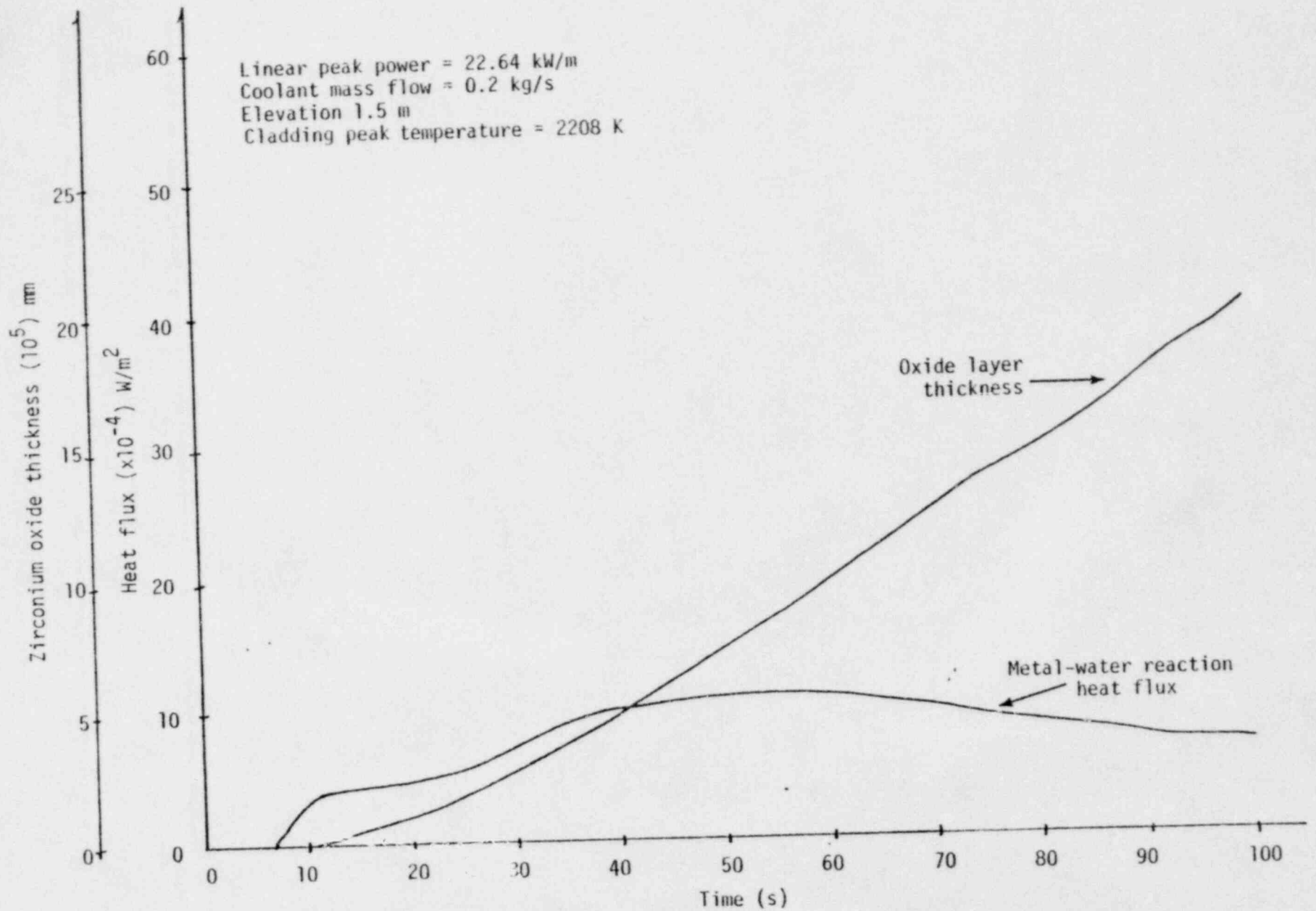


Figure 18. Cladding metal-water reaction heat flux and oxide layer thickness versus time for the steam/water case at the cladding peak temperature elevation.

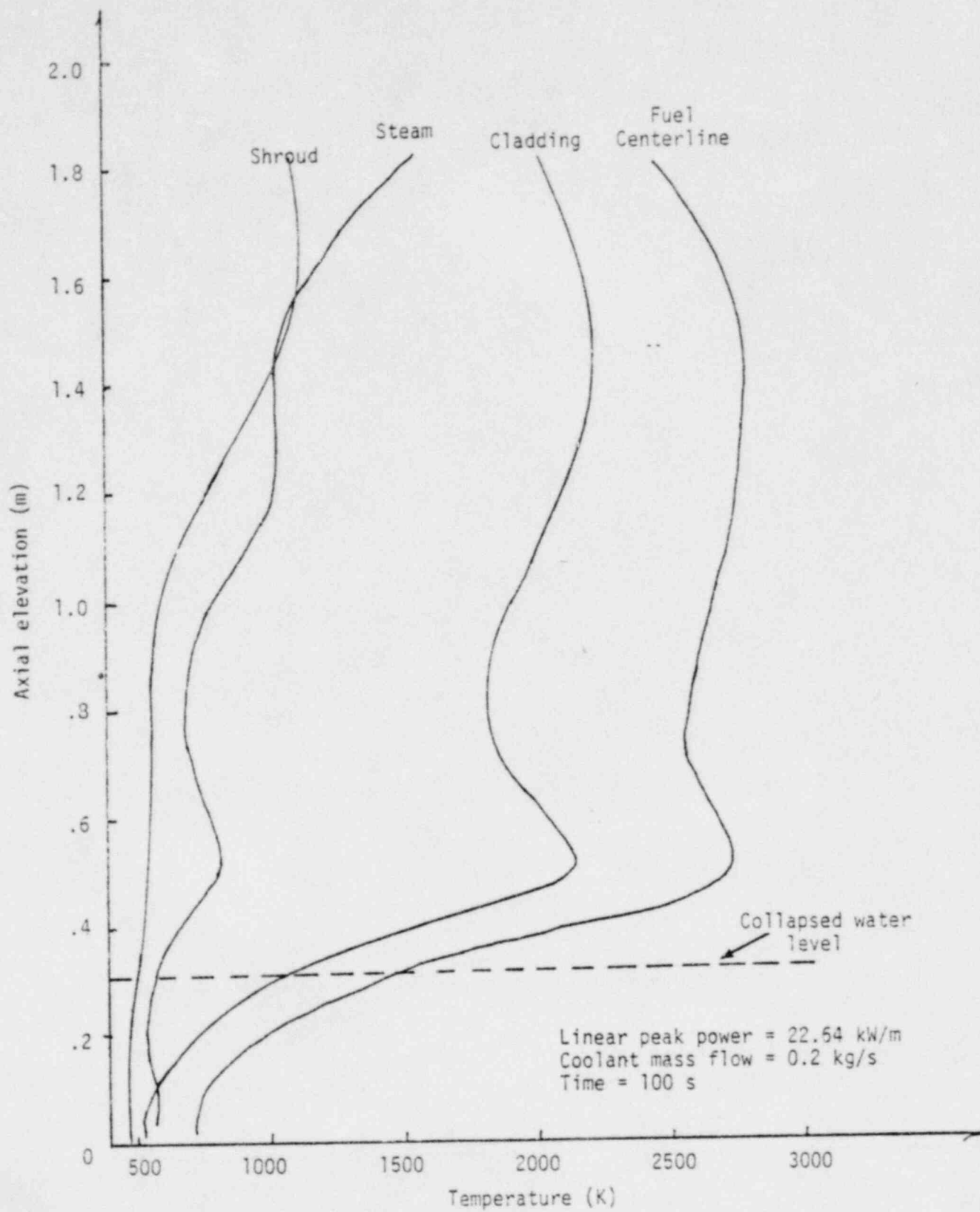


Figure 19. Calculated cladding surface, fuel centerline, steam, and shroud inside surface temperatures versus axial elevation.

conduction out of the bundle. The increasing steam temperatures would then force the fuel rod and shroud temperatures to increase with elevation. Fuel centerline temperatures were predicted to be 400 to 700 K greater than the cladding temperatures along the axial length because of the high fission power required. The predicted fuel centerline peak temperature was about 2800 K, which is about 300 K less than the melting temperature of UO_2 .

As discussed previously, the mode of heat transfer changes radically with axial position within the bundle. Shown in Figure 20 are the rod surface heat transfer coefficients for convection and radiation to both the liquid and vapor, and the void fraction as a function of elevation. The void fraction was initially zero and did not increase until about 0.1 m, above which it rapidly increased to 1.0 at about 1.4 m. The convective heat transfer to liquid rapidly becomes insignificant above 0.2 m, where the void fraction was high. Convection to steam dominated between 0.2 and 0.3 m. Above 0.3 m, the cladding temperature was sufficient to turn on the TRAC radiation heat transfer routine, which at the same time decreased the convective heat transfer coefficient because the radiation component explicitly included in this correlation was eliminated from the calculation. The component of radiation heat transfer from rod to liquid droplets is large in this model, which further tended to increase the rod-to-coolant heat transfer.^a A smooth interpolation does not yet exist in the code for this transition, which, for these particular conditions, resulted in a significant increase in the rod heat transfer, and thus a sudden decrease in the predicted fuel rod temperatures. As the coolant quality approached 1.0 above 0.8 m, the radiation to liquid droplets component of the total heat transfer rapidly became insignificant and cladding temperatures again increased.

a. This component of the TRAC radiation model has not yet been evaluated and it is possible that the absorptivity used for the liquid droplets is too large. If so, this could account for the anomalous predicted behavior.

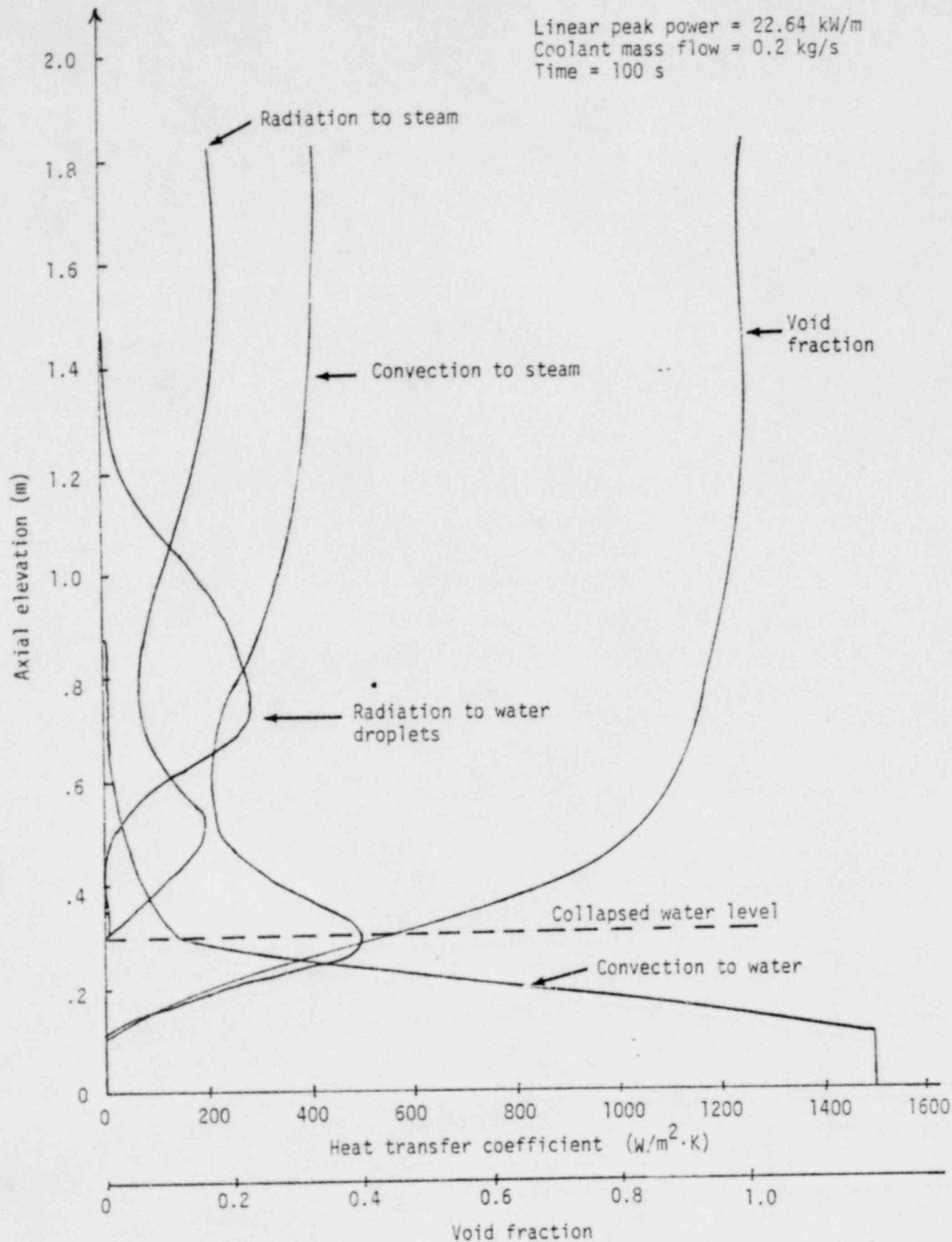


Figure 20. Cladding surface heat transfer coefficients versus axial elevation for the different heat transfer modes and the bundle void fraction.

7. CONCLUSIONS

The TRAC-BDO analyses described in this report indicate that the desired conditions for performing small break LOCA/flow starvation type experiments in the SUPER-SARA circuit in the ESSOR Facility can be attained, with the following considerations:

1. For the steam-filled test space, the desired cladding peak temperatures can be easily attained with a test rod peak power density as low as 3.08 kW/m and a steam mass flow rate of 0.3 m/s. If these low power and mass flow rates lead to difficult operational problems, the power level and flow rate can be increased and the desired conditions can still be attained.
2. For the partially water-filled test space, a minimum test rod peak power density of 15.75 kW/m and a coolant mass flow rate of 0.2 kg/s is required to attain a cladding peak temperature of 1700 K, and a test rod peak power density of 22.64 kW/m is required for the desired cladding temperature of 2300 K. In either case, the desired 1-m water level cannot be maintained, and the maximum water level would be approximately 0.5 m.

REFERENCES

1. Nuclear Safety Analysis Center, Analysis of Three Mile Island-Unit 2 Accident, NSAC-1, July 1979.
2. "SUPER-SARA Programme in ESSOR," Joint Research Center, ES. 2.7700. A. 002, August 1979.
3. EG&G Idaho, Inc., Quarterly Technical Progress Report on Water Reactor Safety Program Sponsored by the Nuclear Regulatory Commission's Division of Reactor Safety Research, October - December 1979, NUREG/CR-1203, EGG-2012, January 1980.
4. Dennis R. Liles et al., TRAC-PIA, An Advanced Best Estimate Computer Program for PWR LOCA Analysis, NUREG/CR-0665, May 1979.
5. J. G. M. Anderson et al., NORCOOL 1, A Model for Analysis of a BWR Under LOCA Conditions, Riso National Laboratory Report NORHAV-D-47, Denmark, August 1977.
6. M. M. Giles, "A Radiation to Steam Model for Reactor Core Thermal Analysis," Proceedings of the Topical Meeting on Thermal Reactor Safety, Sun Valley, Idaho, July 31-August 4, 1977, CONF-770708, Vol. 2, pp. 456-462.
7. N. Zuber and J. A. Findlay, "Average Volumetric Concentration in Two-phase Flow Systems," J. Heat Trans. 87, 453, 1965.
8. M. Ishii, Light-Water-Reactor Research Program, Argonne National Laboratory Report ANL-77-10, October-December 1976.

APPENDIX A

TRAC-BDO CALCULATED SYSTEM AND FUEL ROD VARIABLES

SYSTEM AND FUEL ROD VARIABLES CALCULATED BY THE
TRAC-800 COMPUTER CODE

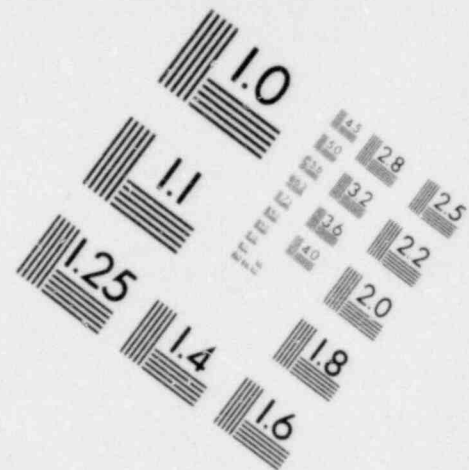
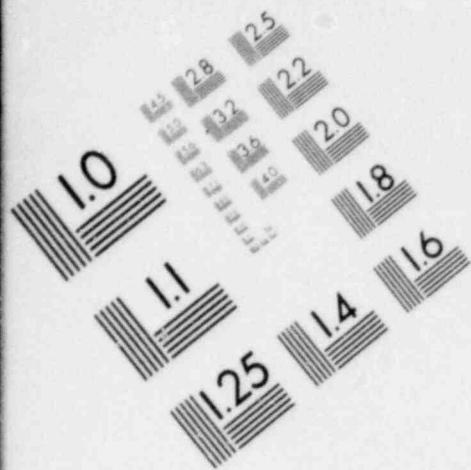
Variable	Identifier	Units
Pressure	Pressure	Pa
Vapor Fraction	Vapor Fraction	Decimal fraction
Saturated Temperature	T SAT	K
Liquid Temperature	T LIQ	K
Vapor Temperature	T VAP	K
Liquid Density	DEN LIQ	Kg/M ³
Vapor Density	DEN VAP	Kg/M ³
Mixture velocity	MIX VEL	M/S
Slip Ratio	SLIP	
Friction Factor	FF	
Leakage Velocity	LEAK VEL	M/S
Channel wall heat transfer mode	IDR (1,2,3,4,6, or 7) ^a	
Channel inside wall convective heat transfer coefficient to liquid	HL	W/M ² K
Channel inside wall convective heat transfer Coefficient to vapor	HV	W/M ² K
Channel inside wall convective heat flux	QFI	W/M ²

a. Heat transfer modes are identified by number as; 1-forced or natural connection to single-phase liquid, 2-nucleate boiling, 3-transition boiling, 4-film boiling, 6-free or forced connection to vapor, 7-forced convection to mixture.

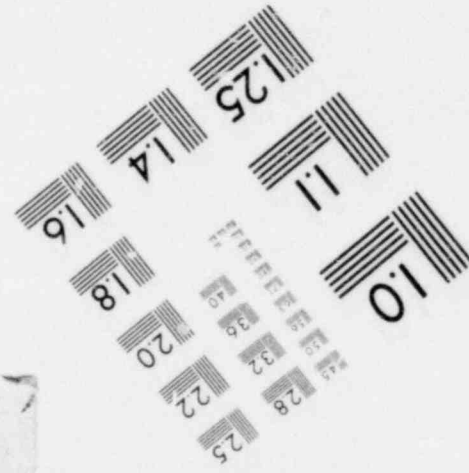
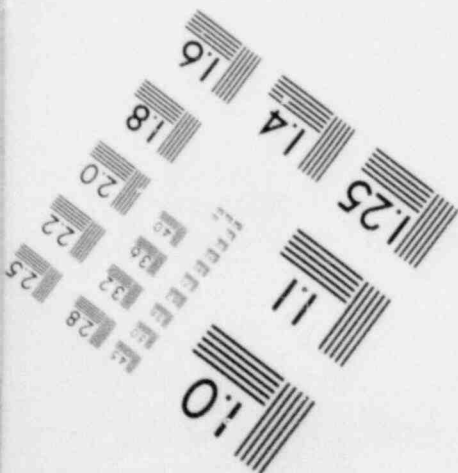
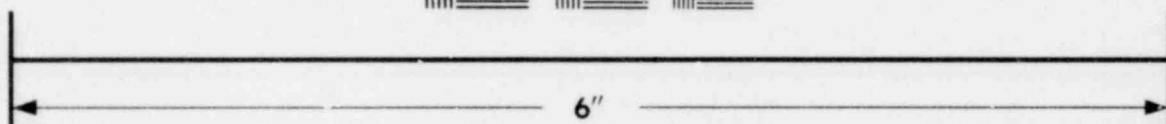
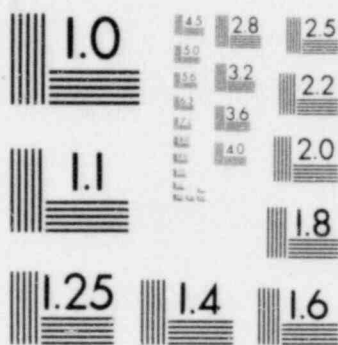
Variable	Identifier	Units
Convective heat transfer coefficient between liquid and vapor	HLV	W/M ² K
Channel outside wall convective heat transfer coefficient to liquid	HLO	W/M ² K
Channel outside wall convective heat transfer coefficient to vapor	HVO	W/M ² K
Channel outside wall convective heat flux	QFO	W/M ²
Channel inside wall radiation heat flux	RAD	W/M ²
Rod heat transfer mode	IHT (1,2,3,4,6, or 7) ^a	
Rod convective heat transfer coefficient to vapor	RDHV	W/M ² K
Rod convective heat transfer coefficient to liquid	RDHL	W/M ² K
Rod surface temperature	RDT	K
Rod convective heat flux	QF	W/M ²

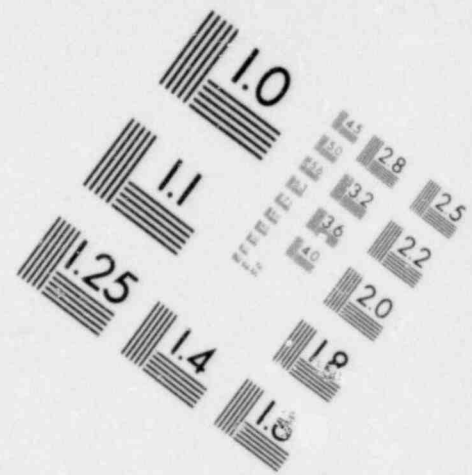
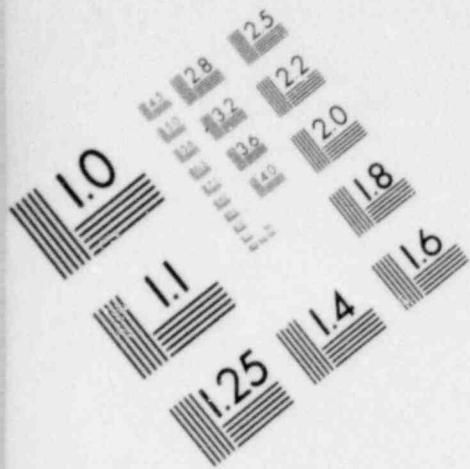
a. Heat transfer modes are identified by number as; 1-forced or natural convection to single-phase liquid, 2-nucleate boiling, 3-transition boiling, 4-film boiling, 6-free or forced convection to vapor, 7-forced convection to mixture.

Variable	Identifier	Units
Rod radiation heat transfer coefficient to liquid	RADHL	W/M ² K
Rod radiation heat transfer coefficient to vapor	RADHV	W/M ² K
Rod radiation heat transfer flux	QRADR	W/M ²
Critical heat flux	QCHF	W/M ²
Critical heat flux temperature	TCHF	K
Axial level of rod	NZ	
Axial level of chan component	CELL	
Metal-water reaction heat flux	QPPMWR	• W/M ²
Thickness of cladding oxidized	DRZN	M

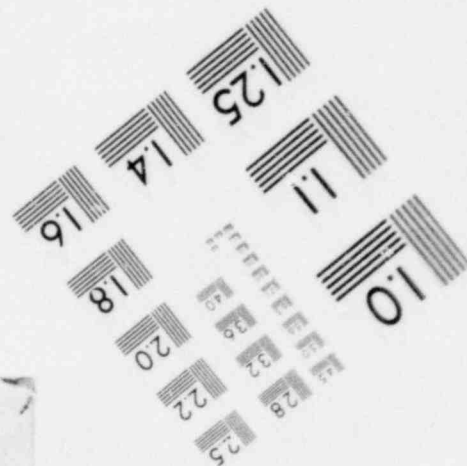
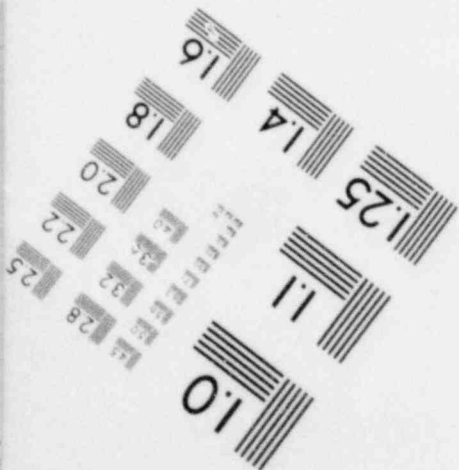
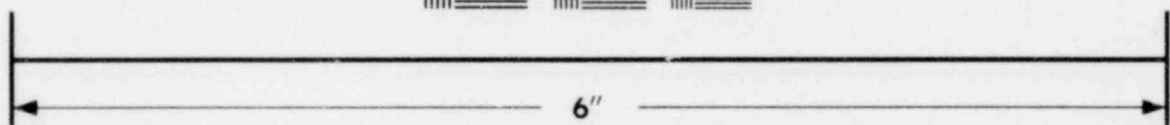
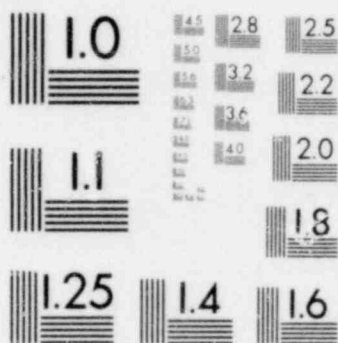


**IMAGE EVALUATION
TEST TARGET (MT-3)**





**IMAGE EVALUATION
TEST TARGET (MT-3)**



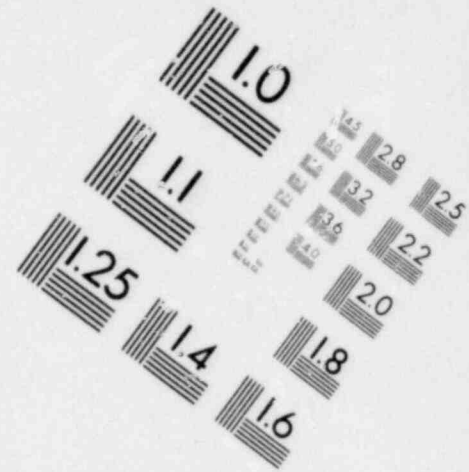
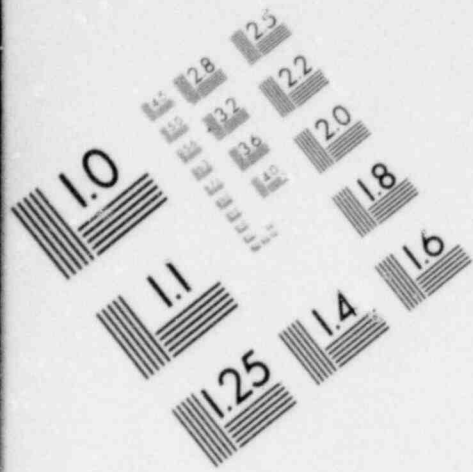
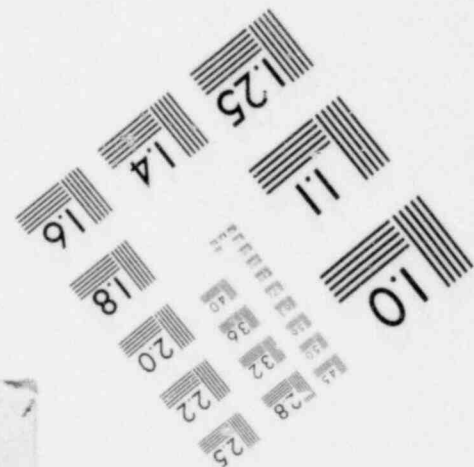
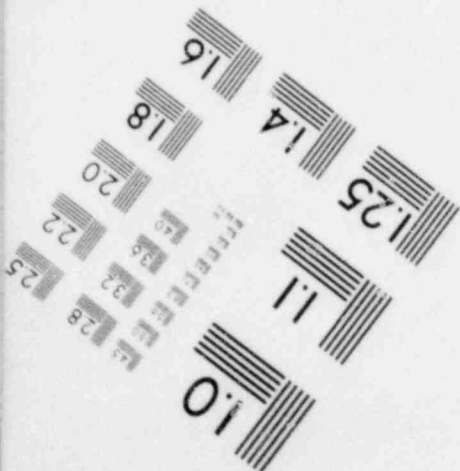
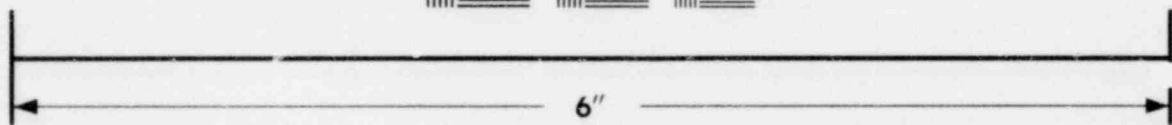
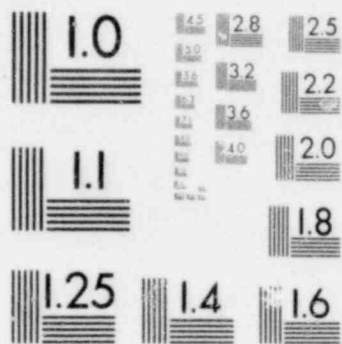
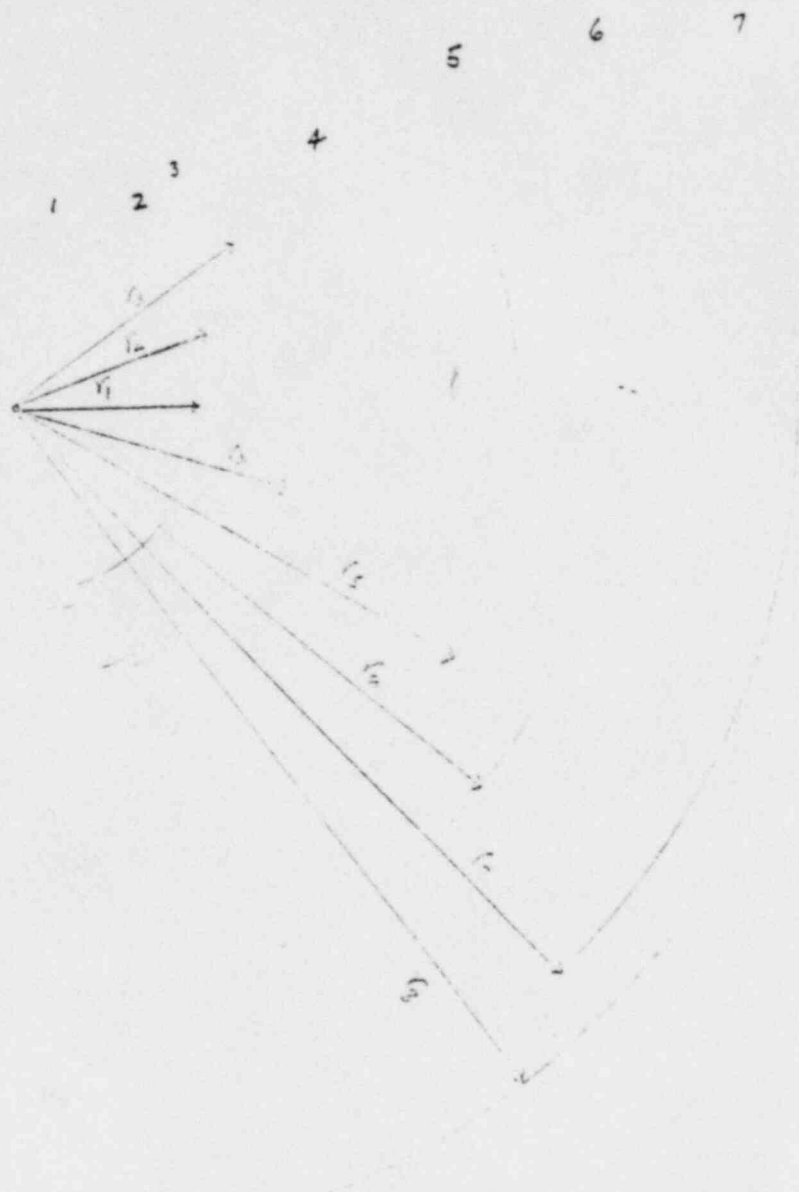


**IMAGE EVALUATION
TEST TARGET (MT-3)**



APPENDIX B

METHOD USED FOR CALCULATING LUMPED PARAMETER HEAT TRANSFER
COEFFICIENT FOR THE SUPER-SARA SMALL BREAK TEST GEOMETRY



- Region 1 : 1.5 mm Zr shroud
- Region 2 : static steam
- Region 3 : 0.8 mm Zr radiation shield
- Region 4 : static steam
- Region 5 : Zr Pressure vessel
- Region 6 : CO₂

- Region 7 : Zr Safety vessel
- $r_1 = 43.72 \text{ mm}$
- $r_2 = 45.22 \text{ mm}$
- $r_3 = 50.18 \text{ mm}$
- $r_4 = 50.98 \text{ mm}$
- $r_5 = 112.8 \text{ mm}$
- $r_6 = 124.3 \text{ mm}$
- $r_7 = 149.0 \text{ mm}$
- $r_8 = 157.1 \text{ mm}$

The over-all heat transfer coefficient

$$U = \frac{1}{(R_1 + R_2 + R_3 + R_4 + R_5 + R_6 + R_7 + R_8) 2\pi r_3 l}$$

$$1. R_1 = \frac{\ln\left(\frac{r_2}{r_1}\right)}{2\pi K_1 l} = \frac{\ln\left(\frac{45.22}{43.72}\right)}{2\pi K_1 l}, \quad l \text{ is the length}$$

where K_1 is the thermal conductivity of region 1 (Shroud).

$$2. R_2 = \frac{\ln\left(\frac{r_3}{r_2}\right)}{2\pi K_2 l} = \frac{\ln\left(\frac{50.19}{45.22}\right)}{2\pi K_2 l}$$

where K_2 is the thermal conductivity of region 2 (steam).

$$3. R_3 = \frac{\ln\left(\frac{r_4}{r_3}\right)}{2\pi K_3 l} = \frac{\ln\left(\frac{50.98}{50.18}\right)}{2\pi K_3 l}$$

where K_3 is the thermal conductivity of region 3 (shield).

$$4. R_4 = \frac{\ln\left(\frac{r_5}{r_4}\right)}{2\pi K_4 l} = \frac{\ln\left(\frac{112.8}{50.98}\right)}{2\pi K_4 l}$$

where K_4 is the thermal conductivity of region 4 (steam).

$$5. R_5 = \frac{\ln\left(\frac{r_6}{r_5}\right)}{2\pi K_5 l} = \frac{\ln\left(\frac{124.3}{112.8}\right)}{2\pi K_5 l}$$

where K_5 is the thermal conductivity of region 5 (Pressure vessel).

$$6. R_6 = \frac{\ln\left(\frac{r_7}{r_6}\right)}{2\pi K_6 l} = \frac{\ln\left(\frac{149}{124.3}\right)}{2\pi K_6 l}$$

where K_6 is the thermal conductivity of region 6 (CO_2).

$$7. R_7 = \frac{\ln\left(\frac{r_8}{r_7}\right)}{2\pi K_7 l} = \frac{\ln\left(\frac{157.1}{149}\right)}{2\pi K_7 l}$$

where K_7 is the thermal conductivity of region 7 (safety vessel).

$$8. R_8 = \frac{1}{2\pi r_8 h_8 l} = \frac{1}{2\pi(0.515) h_8 l}$$

where h_8 is the heat transfer coeff. of safety vessel to D_2O .

$$K_1 = K_3 = K_5 = K_7 = 40 \frac{\text{BTU}}{\text{ft}\cdot\text{hr}\cdot^\circ\text{F}}$$

$$K_2 = K_4 = 0.032 \frac{\text{BTU}}{\text{ft}\cdot\text{hr}\cdot^\circ\text{F}}$$

$$* K_6 = 0.0025 \frac{\text{BTU}}{\text{ft}\cdot\text{hr}\cdot^\circ\text{F}}$$

$$** h_8 = 41.52 \frac{\text{BTU}}{\text{ft}^2\cdot\text{hr}\cdot^\circ\text{F}}$$

* K_c calculations:

CO_2 gas forced convection - $\sim 100^\circ\text{F}$

$$\rho = 0.108 \frac{\text{lbm}}{\text{ft}^3}, \quad \nu = 0.098, \quad k = 0.01 \frac{\text{BTU}}{\text{hr}\cdot\text{ft}\cdot^\circ\text{F}}$$

$$N_{Pr} = 0.77, \quad \dot{m} = 2.2 \frac{\text{lbm}}{\text{s}} \Rightarrow V = 14.8 \frac{\text{ft}}{\text{s}}$$

$$N_{REL} = \frac{Vl}{\nu} = \frac{14.8 \times 6}{0.098} = 906.34$$

$$N_{NUL} = 0.664 (N_{REL})^{1/2} (N_{Pr})^{1/3}$$

$$= 0.664 (906.34)^{1/2} (0.77)^{1/3}$$

$$= 0.664 (30.1)(0.92)$$

$$= 18.32$$

$$h_s = N_{NUL} \frac{k}{l} = 18.32 \frac{0.01}{6} = \underline{\underline{0.0305}} \frac{\text{BTU}}{\text{hr}\cdot\text{ft}\cdot^\circ\text{F}}$$

$$\left(\text{Since } N_{NUL} = \frac{hl}{k} \right)$$

$$\text{Therefore, } k_c = 0.0305 \times 0.081 = 0.0025 \frac{\text{BTU}}{\text{hr}\cdot\text{ft}\cdot^\circ\text{F}}$$

→ h_g Calculations for D20

Free convection, mean film temperature = $\frac{158 + 122}{2}$
 $= 140^\circ F$

$\rho = 61.39 \text{ lbm/ft}^3$, $\mu = 1.14 \text{ lbm/ft-hr}$

$\nu = 0.0186 \text{ ft}^2/\text{hr}$, $K = 0.378 \text{ BTU/hr-ft-}^\circ F$

$\beta = 0.29 \times 10^{-3} \text{ 1/}^\circ R$, $N_{Pr} = 3.01$

$$N_{GrL} = \frac{g L^3 \rho \Delta t}{\nu^2} = \frac{(6)^3 (32.2) (61.39) (3600) (0.29 \times 10^{-3})}{(1.14)^2}$$

$(158-122)$

$$= 4.45 \times 10^{10}$$

So $N_{GrL} \times N_{Pr} = 4.45 \times 10^{10} \times 3.01 = 1.34 \times 10^{11}$

$$N_{NuL} = 0.129 (1.34 \times 10^{11})^{1/3}$$

$$= 0.129 (134)^{1/3} (10)^3$$

$$= 659$$

$\therefore h_g = 659 \frac{0.378}{6} = 41.52 \text{ BTU/ft}^2\text{-hr-}^\circ F$

$$\therefore U = \frac{1}{\frac{r_8 \ln\left(\frac{45.22}{43.72}\right)}{K_1} + \frac{r_8 \ln\left(\frac{50.19}{45.22}\right)}{K_2} + \frac{r_8 \ln\left(\frac{50.99}{50.19}\right)}{K_3}}$$

$$\frac{r_8 \ln\left(\frac{112.8}{50.98}\right)}{K_4} + \frac{r_8 \ln\left(\frac{124.3}{112.8}\right)}{K_5} + \frac{r_8 \ln\left(\frac{149}{124.3}\right)}{K_6}$$

$$\frac{r_8 \ln\left(\frac{157.1}{149}\right)}{K_7} + \frac{1}{h_g}$$

$$= \frac{1.94}{\frac{0.0337}{40} + \frac{0.1041}{0.032} + \frac{0.00158}{40} + \frac{0.794}{0.032} + \frac{0.0971}{40}}$$

$$\frac{0.18125}{0.0025} + \frac{0.053}{40} + \frac{1}{41.52}$$

$$= \frac{1.94}{0.00084 + 3.253 + 0.0000395 + 24.8 + 0.002428}$$

$$\frac{1.94}{72.5 + 0.001325 + 0.0241} = \frac{1.94}{100.582} = 0.0193 \text{ BTU/hr-ft}^2\text{-}^\circ\text{F}$$

$$\therefore U = 0.0193 \text{ BTU/hr-ft}^2\text{-}^\circ\text{F} = 0.1095 \text{ W/m}^2\text{K}$$

$$\text{The } K_{\text{eff}} = 0.1095 \times .1134 = 0.0124 \frac{\text{w}}{\text{mk}}$$